NASA
Technical
Paper
3079

February 1991

Radiation Protection for Human Missions to the Moon and Mars

Lisa C. Simonsen
and John E. Nealy

NASA

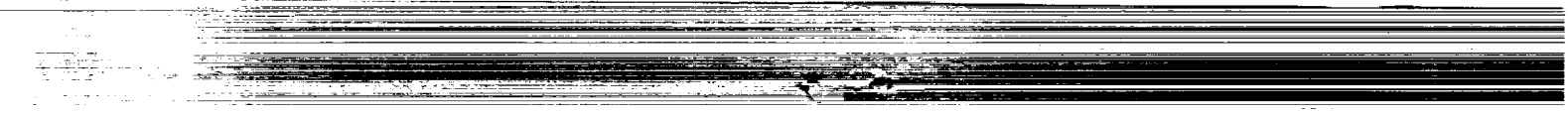

NASA Technical Paper 3079

1991

Radiation Protection for Human Missions to the Moon and Mars

Lisa C. Simonsen
and John E. Nealy
Langley Research Center
Hampton, Virginia

National Aeronautics and Space Administration
Office of Management
Scientific and Technical Information Division

Summary

Radiation protection assessments are performed for advanced lunar and Mars manned missions. The Langley cosmic ray transport code and the Langley nucleon transport code are used to quantify the transport and attenuation of galactic cosmic rays and solar proton flares through various shielding media. Galactic cosmic radiation at solar maximum and minimum conditions, as well as various flare scenarios, is considered. Propagation data for water, aluminum, liquid hydrogen, lithium hydride, lead, and lunar and Martian regolith (soil) are included. Shield thickness and shield mass estimates required to maintain incurred doses below 30-day and annual limits (as set for Space Station Freedom and used as a guide for space exploration) are determined for simple-geometry transfer vehicles. Dose estimates are also presented for candidate lunar base habitats shielded with lunar regolith. On the surface of Mars, dose estimates are presented both for crews having the carbon dioxide atmosphere as their only protection and for crews protected by additional shielding provided by Martian regolith for a candidate habitat.

Introduction

One of the next major space endeavors will be the human exploration of the Moon and Mars as described in the *Report of the 90-Day Study on Human Exploration of the Moon and Mars.*[1] The most critical aspect of these missions is the safety and health of the crew. One of the major health concerns is the damaging effects of ionizing space radiation. Once the crew leaves the Earth's protective environment, they will be bombarded by radiation of varying energies and ranges of intensity. The most harmful components of this radiation are trapped electrons and protons in the Van Allen belts, solar flare protons, and galactic cosmic rays. Adequate shielding will be required to protect the crew from this environment.

Astronaut doses incurred from the Van Allen belts highly depend on the time spent in the high-flux regions of the belt and the state of the fields at the time of exposure. Large temporal variations are observed in the outer zone of the belts in which a dose incurred over a short time period may increase by an order of magnitude or more (Wilson 1978). The nature of the energy spectrum is such that crew members in a thinly shielded spacecraft can incur very large doses. However, moderate shielding (approximately 2–5 g/cm^2) and single passes through the belts usually result in relatively small delivered doses (<1 rem) under normal field conditions. These doses are of most concern for low Earth orbits to geostationary orbits and for spiraling trajectories through the belts.

Once outside of the influence of the Earth's magnetic field, the astronauts will be constantly bombarded by galactic cosmic radiation (GCR). The constant bombardment of these high-energy particles delivers a steady dose. The intensity of the GCR flux varies over the 11-year solar cycle. The maximum dose received will occur at solar minimum. For the long-duration missions, this dose can become career limiting. Thus, the amount of shielding required to protect the astronauts will depend on the time and duration of the mission.

Anomalously large solar proton events are relatively rare with one or two events per solar cycle. The largest flares observed in the past are the November 1949, the February 1956, the November 1960, and the August 1972 events. Solar cycle XXI (1975–1986) proved relatively quiet with no unusually large events. However, with the onset of cycle XXII, new concern has arisen with several large events occurring in the later half of 1989. A solar flare event can be very dangerous if a spacecraft is inadequately shielded because flares can deliver a very high dose in a short period of time. For relatively short-duration missions (2–3 months), the most important radiation hazard is the possibility of an unusually large solar proton event. The amount of shielding required for protection will depend on the nature of the energy spectrum of the flare and the intensity of the event.

Shielding must be provided to maintain crew-incurred doses to an acceptable level. Currently there

[1]This is a limited-distribution report compiled by NASA in November 1989 (referred to herein as "The 90-Day Study").

are no limits established for exploratory class missions; however, it is recommended that limits established for low-Earth-orbit operations be used as guidelines (NCRP-98, 1989). These limits are established by the National Council on Radiation Protection and Measurement and include dose limits for the skin, ocular lens, and vital organs (NCRP-98, 1989). For high-energy radiation from galactic cosmic rays and solar proton flares, the dose delivered to the vital organs is the most important with regard to latent carcinogenic effects. This dose is often taken as a whole body exposure and is assumed equal to the blood-forming-organ (BFO) dose. When detailed body geometry is not considered, the BFO dose is usually computed as the dose incurred at a 5-cm depth in tissue (simulated by water in these analyses). Dose-equivalent limits are established for short-term (30-day) exposures, annual exposures, and total career exposure. These values are listed in table 1. Short-term exposures are important when considering solar flare events because of their high dose rate. Doses received from GCR on long-duration missions are especially important to total career limits, which are determined by the age and gender of the individual. For instance, career limits for typical male and female astronauts who are 30 years old at the time of their first exposure are 200 rem and 140 rem, respectively.

Table 1. Dose-Equivalent Limits Recommended for United States Astronauts in Low Earth Orbit

Exposure time	Vital organ, rem	Ocular lens, rem	Skin, rem
Career	[a]100 400	400	600
Annual	50	200	300
30 days	25	100	150

[a]Varies with age and gender.

Current mission scenarios for the Nation's Human Exploration Initiative are described in The 90-Day Study. The final goal of the Initiative is to establish operational outposts on both the Moon and Mars. After a 3-day trip from Earth to the Moon, crew-rotation times on the surface are described as starting with a 30-day stay, growing to a 6-month stay, to a 12-month stay, and finally growing to 600 days. The flight time to Mars is estimated to take from 7 months to over a year each way. Crew times on the Martian surface are described as starting with a 30-day stay, growing to a 90-day stay, and finally up to a 600-day stay. Thus, an entire Mars mission is estimated to take anywhere from 500 to 1000 days round trip. Different shielding strategies will exist for each phase of each lunar and Martian mission. Free-space shielding requirements for lunar transfer vehicles will differ greatly from those selected for the Mars vehicles because of the large differences in travel time. Likewise, planetary habitation-shielding strategies utilizing local resources will differ greatly from the transfer vehicles. Habitation shielding on the lunar surface versus that on the Martian surface will also differ greatly because of the differences in their environments.

Symbols and Abbreviations

AE-8, AP-8	standard trapped electron and proton environment models
AU	astronomical unit
BFO	blood-forming organ
BRYNTRN	a baryon transport code
CREME	cosmic ray effects on microelectronics
ECCV	Earth capture control vehicle
GCR	galactic cosmic radiation
GOES	Geostationary Operational Environmental Satellite
IMP	Interplanetary Monitoring Platform
LET	linear energy transfer
NOAA	National Oceanic and Atmospheric Administration
NRL	Naval Research Laboratory
NTC	Nucleon Transport Code
Q	quality factor
RCS	reaction control system
t	thickness
ρ	density, g/cm^3

Radiation Environment

The free-space radiation environment comprises numerous particles with various energy spectra as shown in figure 1 (Wilson 1978). The particles of relatively high energy and fluxes are of the most concern. The galactic cosmic rays are the most penetrating because of their higher energies. Additionally, the large fluxes associated with major flare events make them potentially lethal. Very long periods of time in the inner zone of the Van Allen belts can be as potentially dangerous as a large flare event. However, for missions involving long times outside the Earth's magnetosphere, radiation-protection requirements will be dictated primarily by the solar flare and galactic cosmic ray environment.

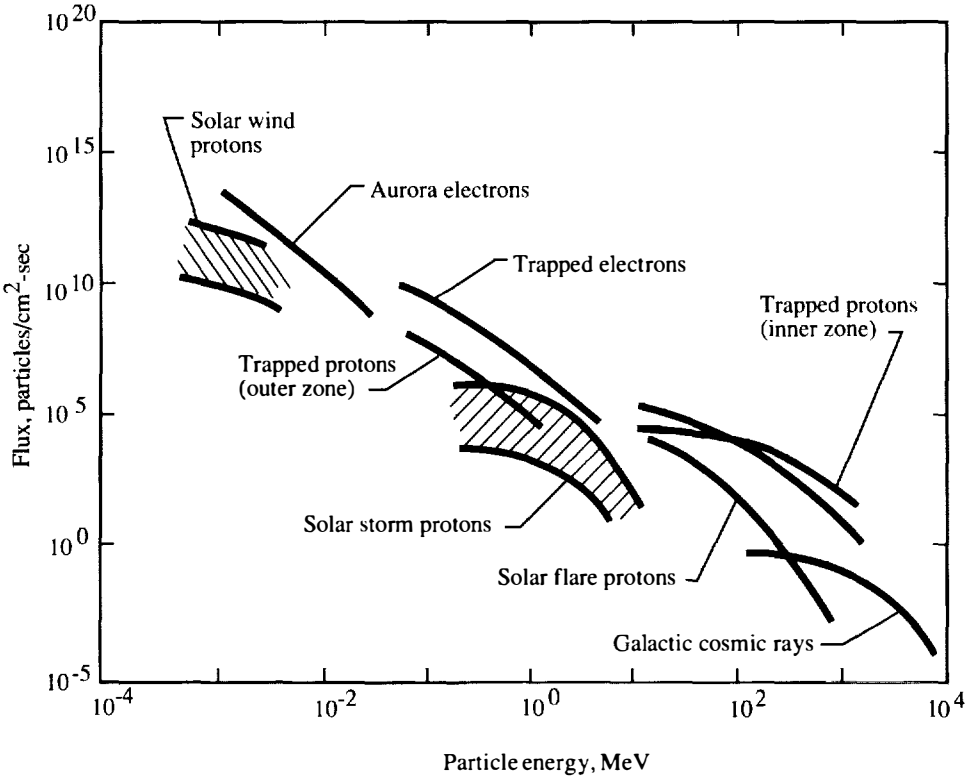

Figure 1. Free-space radiation environment (Wilson 1978).

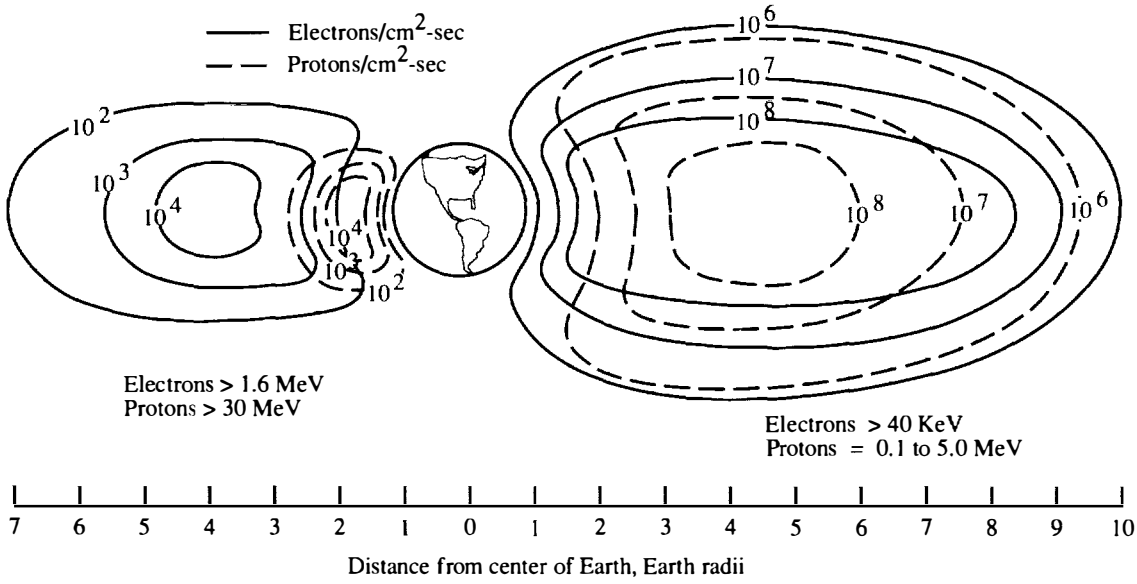

Figure 2. Near-Earth trapped radiation and solar proton environment (Parker and West 1973). For clarity, low-energy integral fluxes are shown only on the right and high-energy fluxes are shown only on the left.

Substantial contributions to our knowledge of the free-space radiation environment have been made by ground-based measurements. When these measurements are coupled with the more recent and comprehensive data provided by manned and unmanned spacecraft, sufficient data exist from which a variety of environmental models can be derived. Several models have become practical standards for

radiation-exposure applications. For the trapped protons and electrons in the geomagnetic field, the AP-8 and AE-8 models of the NASA Goddard Space Flight Center are widely used (Gaffey and Bilitza 1990). For the solar flare protons, many studies utilize individual spectra of observed large flares (Nealy et al. 1988; Simonsen et al. 1990a; Townsend et al. 1989). For the galactic cosmic rays, a model developed at the Naval Research Laboratory is frequently implemented for the heavy-ion environment (Adams et al. 1981).

Van Allen Belts

A semiquantitative pictorial of the distributions of trapped protons and electrons in the Van Allen belts is shown in figure 2 (Parker and West 1973). The distributions of the charged particles with low-energy integral fluxes are shown on the right-hand side of the figure, which indicates the approximate extent of the regions with substantial total particle flux. The left-hand side of figure 2 gives the integral fluxes of particles with higher energies, for which the "inner" and "outer" belt distinctions are prominent. For moderately shielded spacecraft (approximately 5 g/cm^2), such as those contemplated for advanced missions, doses incurred during transit through the trapped belts are not significant compared with the anticipated free-space contributions. However, substantial cumulative exposures in the belts will result for sustained operations in low Earth orbit (LEO) at altitudes greater than approximately 400 km. In addition, conceptual multiple-pass trajectories spiraling through the trapped regions may also result in significant doses. Generally, the exposures due to the natural environment for long-duration missions will result from solar flare protons and GCR heavy ions.

Solar Flare Events

The three large solar flares of August 1972, November 1960, and February 1956 are widely used to estimate flare shielding requirements. The fluence-energy spectra for these events are shown in figure 3 (Wilson 1978). The flare of August 1972 produced the greatest number of protons above 10 MeV, but it had fewer protons than the other two events for energies greater than approximately 150 MeV. The February 1956 event produced approximately one-tenth as many protons above 10 MeV as the 1972 flare, but it delivered far more protons of 200 MeV or greater than the two other flares. The November 1960 flare spectrum exhibited intermediate characteristics.

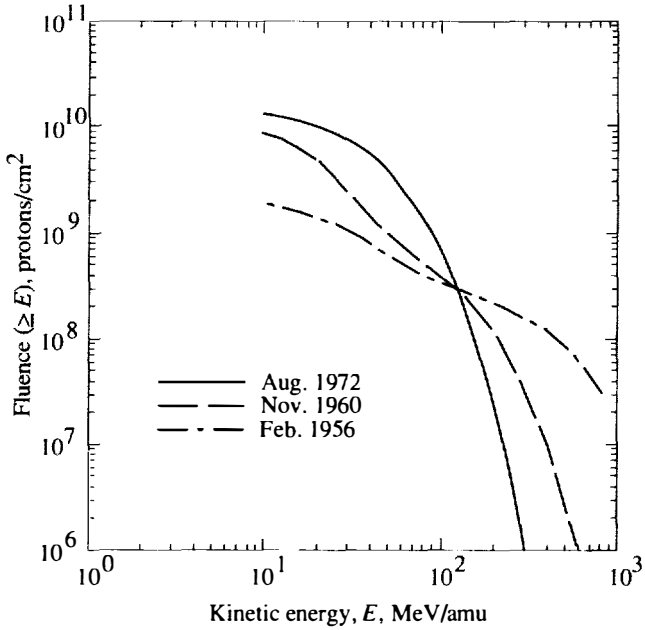

Figure 3. Integrated fluence spectra for three large solar proton flares (Wilson 1978).

Solar cycle XXI (1975–1986) was relatively quiet with no flare events of these magnitudes recorded. The flares of cycle XXI may constitute the typical proton fluence within a solar cycle because of the more normally occurring small- and medium-sized events. The proton fluxes due to flare events were measured by particle monitors onboard the Interplanetary Monitoring Platform (IMP) satellites, IMP-7 and IMP-8. Fifty-five flares within solar cycle XXI were measured to have integral fluences greater that 10^7 protons/cm^2 for energies greater than 10 MeV. The other flares of lower fluence and energy would contribute negligibly to dose calculations. Figure 4(a) shows the integral fluences of the 55 flares as they are distributed in time throughout the cycle, and figure 4(b) shows the fluence spectra for each of these flares (Goswami et al. 1988).

With the onset of solar cycle XXII (1986–1997), several flares larger than any recorded in cycle XXI have already occurred in the months of August through December 1989. Six flares occurring in this time frame have been recorded by the GOES-7 satellite. Figure 5 shows the proton fluence energy spectra based on rigidity functions reported by Sauer et al. (1990). The magnitude of the October 1989 event is on the same order as the August 1972 event and has heightened concern over flare shielding strategies. The addition of these six flares can provide a fairly realistic estimate of a flare environment that may be encountered during missions taking place in the 5 or 6 years of active Sun conditions.

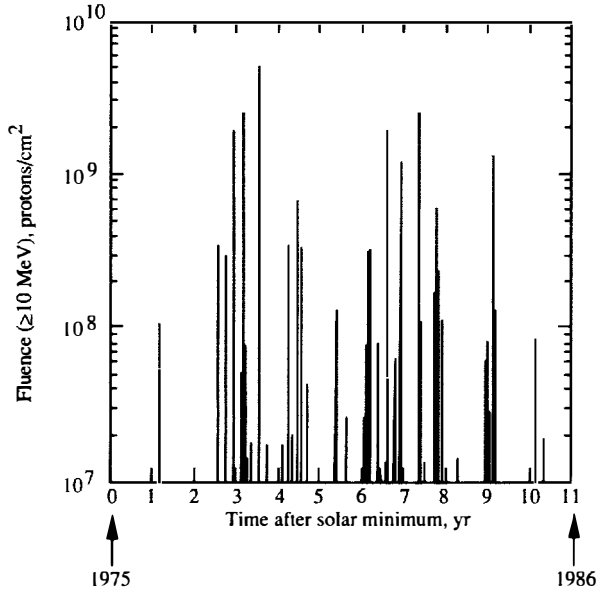

(a) Integral fluence.

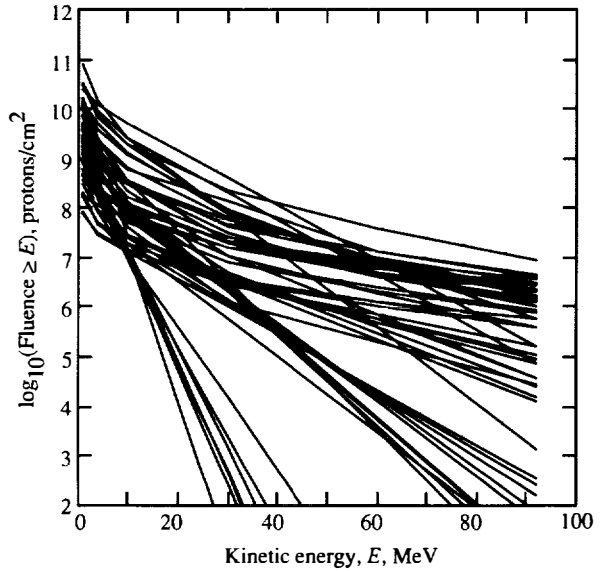

(b) Fluence spectra.

Figure 4. Solar proton flares during solar cycle XXI (1975–1986) (Goswami et al. 1988).

Galactic Cosmic Radiation

Galactic cosmic radiation consists of the stripped nuclei of the chemical elements that have been accelerated to extremely high energies outside the solar system. Measurements have been made to specify a working model of these distributions. Considerable uncertainty exists in the energy distributions of these ions. The natural GCR environment used in these analyses is the widely used Naval Research Laboratory (NRL) CREME model, which specifies ion fluxes for particles of atomic numbers *(Z)* between 1 and 28 (hydrogen through nickel) (Adams et al. 1981). Figure 6 shows the GCR particle spectra at solar minimum conditions, when the fluxes are the greatest because of the decreased modulation of the interplanetary magnetic field. Figure 7 indicates the nature of the flux reduction at solar maximum conditions according to the NRL model, where the flux decrease is most prominent for energies below approximately 10^4 MeV. There is growing evidence that the NRL model overestimates the modulation effect. The particle fluxes are seen to vary between solar minimum and maximum by roughly a factor of 2. The rather comprehensive study of ground level measurements by Nagashima et al. (1989) indicates an approximate sinusoidal behavior of the general cosmic ray intensity between the extrema within a cycle.

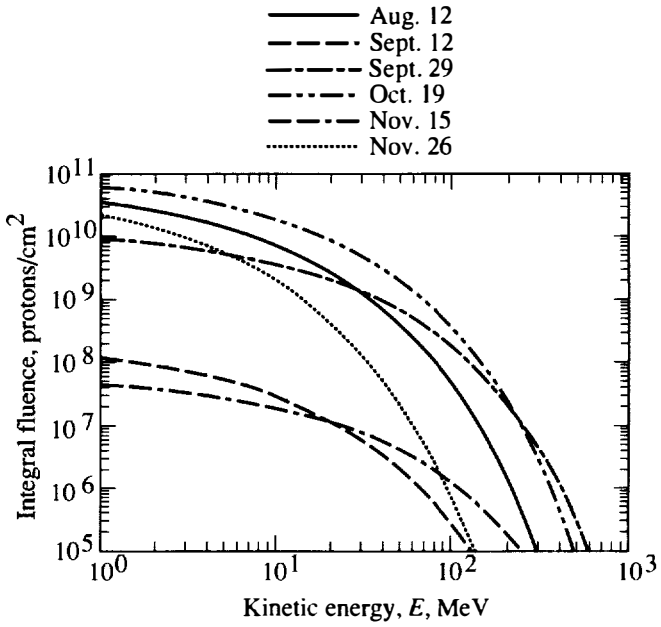

Figure 5. Six large solar flare integral fluences based on 1989 GOES-7 data (Sauer et al. 1990).

Analysis

The analyses presented here will focus on the shielding requirements for GCR and different flare scenarios. Shielding thicknesses selected for these missions should also reduce doses incurred from the Van Allen belts to a negligible amount provided that long times are not spent in the belts.

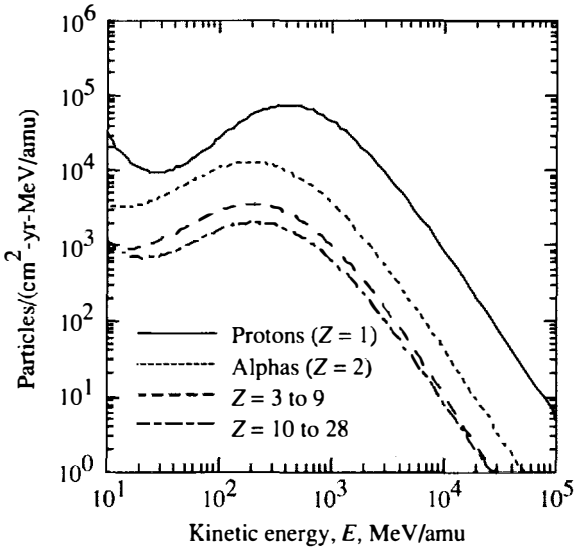

Figure 6. Ion spectra of galactic cosmic ray for solar minimum conditions (Adams et al. 1981).

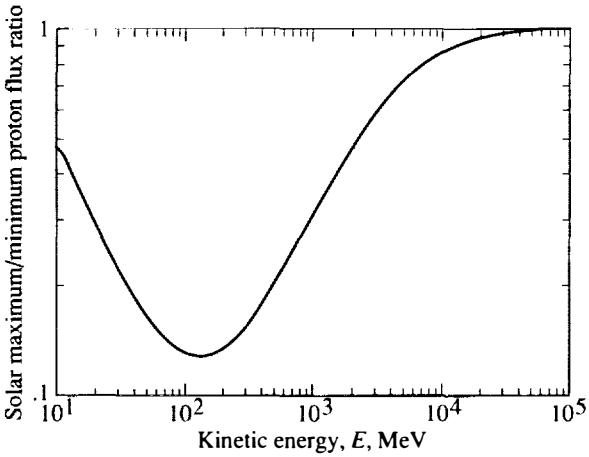

Figure 7. GCR proton flux reduction factors at solar maximum conditions (Adams et al. 1981).

Transport Codes

The NASA Langley Research Center nucleon and heavy-ion transport computer codes are used to predict the propagation and interactions of the free-space nucleons and heavy ions through various media. For large solar flare radiation, the baryon transport code (BRYNTRN) is used (Wilson et al. 1989). For the galactic cosmic rays, an existing heavy-ion transport code is integrated with the BRYNTRN code to include the transport of high-energy heavy ions up to atomic number 28 (Wilson et al. 1986, 1987; Townsend et al. 1990a). Both codes solve the fundamental Boltzmann transport equation in the one-dimensional, or "straight ahead," approximation form:

$$\left[\frac{\partial}{\partial x} - \frac{\partial}{\partial E}S_j(E) + \mu_j(E)\right]\Phi_j(x,E) = \sum_{k>j}\int_E^\infty \sigma_{jk}(E,E')\Phi_k(x,E')\,dE'$$

where the quantity to be evaluated, $\Phi_j(x,E)$, is the flux of particles of type j having energy E at spatial location x. The solution methodology of this integrodifferential equation may be described as a combined analytical-numerical technique (Wilson 1977). The accuracy of this numerical method has been determined to be within approximately 1 percent of exact benchmark solutions (Wilson and Townsend 1988a). The data required for solution consist of the stopping power S_j in various media, the macroscopic total and absorption nuclear cross sections μ_j, and the differential nuclear interaction cross sections σ_{jk}. The differential cross sections describe the production of type j particles with energy E by type k particles of energies $E' > E$. Detailed information on these data base compilations is described in references by Wilson et al. (1988b, 1989) and Townsend and Wilson (1985).

In addition to benchmark solution checks on the numerical precision of the code, a comparison with standard Monte Carlo type calculations has also been made (Shinn et al. 1990). A sample of BRYNTRN results compared with results from the statistical Nucleon Transport Code (Scott and Alsmiller 1968) is shown in figure 8 where the dose values are given for a 30-cm tissue layer behind an aluminum shield of 20 g/cm^2. The input spectrum used is expressed analytically with the integral fluence F as a function of proton rigidity R:

$$F(>E) = C_o \exp\left[\frac{-R(E)}{R_o}\right]$$

with R_o equal to 100 MV and C_o chosen so that F(30 MV) equals 10^9 protons/cm^2. Such a function is representative of a large proton event, and it is seen that the BRYNTRN results show excellent agreement with the Monte Carlo calculations.

The present GCR code formulation is considered to be an interim version since some features of the transport interaction phenomena have yet to be incorporated. These include improvements and additions to the existing nucleus-nucleus cross sections and their energy dependence and provisions for pion and muon contributions. Further improvements in target fragmentation treatment and computational efficiency are to be incorporated even though

computational execution times are already faster than counterpart statistical (Monte Carlo) calculations. These improvements should not greatly alter the current results, and the present interim version of the GCR code should provide a reasonable description of cosmic ray particle fluxes and the corresponding dose predictions. Many uncertainties presently exist in high-energy, heavy-ion transport analyses; therefore, the results included herein should be considered as current state-of-the-art "best estimates."

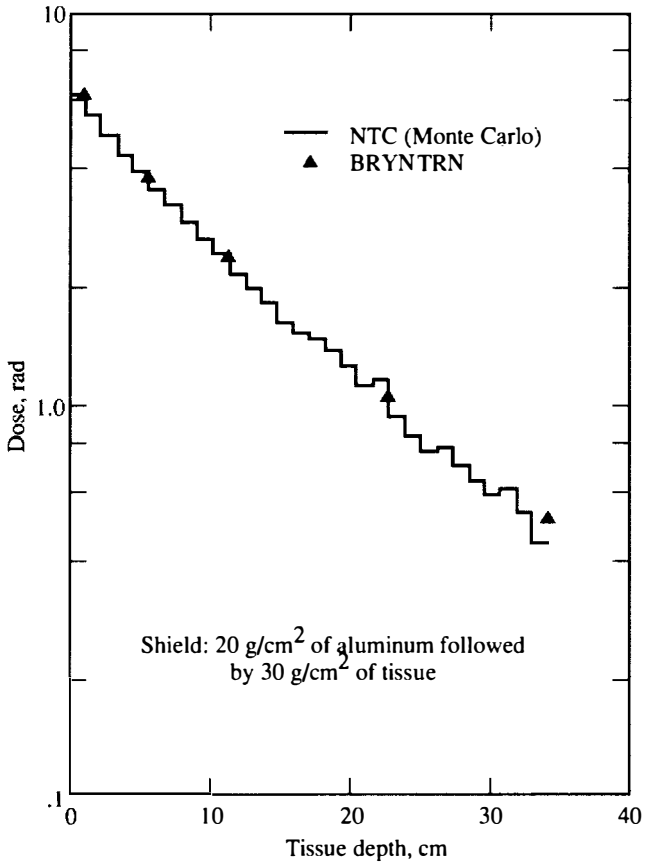

Figure 8. Comparison of results from BRYNTRN with equivalent Monte Carlo calculations (Shinn et al. 1990).

The absorbed dose D due to energy deposition at a given location x by all particles (in units of rad) is calculated according to

$$D(x) = \sum_j \int_0^\infty S_j(E)\ \Phi_j(x,E)\ dE$$

The degree to which biological systems undergo damage by ionizing radiation is not simply proportional to this absorbed dose for all particle types. For human exposure, the dose equivalent is defined by introducing the quality factor Q which relates the biological damage incurred due to any ionizing radiation to the damage produced by soft X rays. (See ICRU-40, 1986, and ICRP-26, 1977, for further discussion.) In general, Q is a function of linear energy transfer, which in turn is a function of both particle type and energy. For the present calculations, the quality factors used are those specified by the International Commission on Radiological Protection (ICRP-26, 1977). The values of dose equivalent H (in units of rem) are computed as

$$H(x) = \sum_j \int_0^\infty Q_j(E)\ S_j(E)\ \Phi_j(x,E)\ dE$$

These are the values used to specify radiation-exposure limits for carcinogenic and mutagenic effects. (See table 1). (The skin dose can be used to approximate the dose to the ocular lens; however, the estimate is somewhat conservative with respect to lens opacity and cataract formation.)

Propagation Data

The BRYNTRN code and the combined nucleon/heavy-ion transport code are easily applied to various media. The GCR and solar flare energy distributions (figs. 3, 4(b), 5, and 6) are input into the code as the initial particle fluxes at the media boundaries. Results include slab calculations of the particle-flux energy distributions at various absorber amounts from which slab-dose estimates as a function of absorber amount are determined. The slab calculations correspond to a monodirectional beam of particles normally incident on a planar layer of shield material. For the straight-ahead transport approximation, the dose at a specific slab-shield depth with normal incident radiation is equivalent to the dose in the center of a spherical-shell shield of the same thickness in a field of isotropic radiation. This is depicted in figure 9.

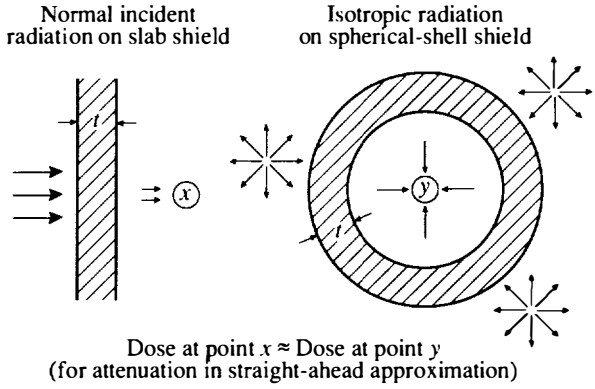

Figure 9. Calculation equivalence of slab shield and spherical-shell shield.

Basic propagation data have been generated for a variety of materials for both the GCR spectrum

and different flare spectra. The propagation results are displayed as dose versus absorber amount or areal density (in units of g/cm^2) which can be converted to a linear thickness by dividing by density. Displaying results in this manner is helpful in comparing the shield effectiveness of various materials because equal absorber amounts for a given shielded volume will yield equal shield masses even though their linear thicknesses may differ.

For incident solar flare protons, the variation of dose with shield amount is sensitive to the energy characteristics (differential flux spectra). Figure 10 illustrates the BFO dose as a function of thickness in aluminum followed by a 5-cm tissue layer for the three flares whose spectra are shown in figure 3. For these flares, the proton fluences have an approximate coincidence close to 100 MeV. Consequently, this behavior is reflected in a corresponding crossover of the dose-depth curves of figure 10, where the coincidence occurs at approximately 15 g/cm^2 of aluminum.

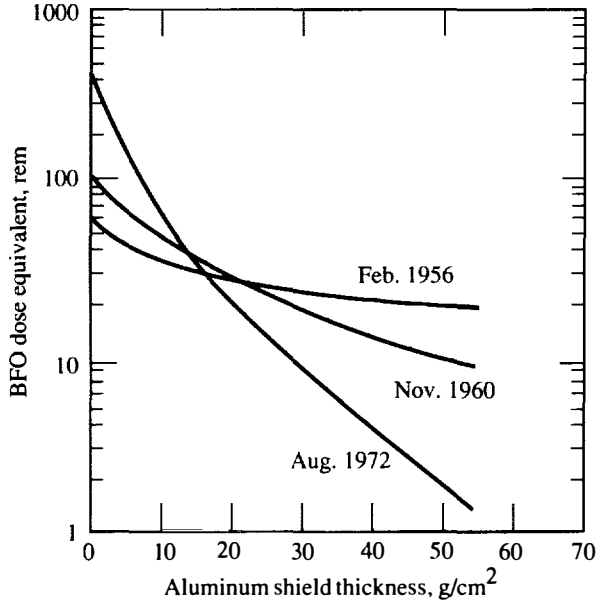

Figure 10. BFO dose equivalent as a function of aluminum shield thickness for three large solar flare events (Townsend et al. 1989). (1 g/cm^2 of aluminum is equivalent to 0.37 cm thickness.)

The combined fluences of the solar proton events occurring in the latter part of 1989 (fig. 5) have spectral characteristics similar to the August 1972 event. The BFO dose as a function of thickness for several shield materials is shown in figure 11 for this flare scenario. On a per-unit-mass basis, water and lithium hydride have almost identical shield-effectiveness properties for all shield thicknesses. Such similarities apply as well to media of low atomic weight and high hydrogen content (e.g., hydrocarbon polymers) which may be used as bulk shields. The curves for aluminum and lead are indicative of the decreasing relative effectiveness of higher atomic weight media. This effect can be attributed to the differences in proton stopping powers of the materials and to the greater numbers of secondary nucleons generated in the heavier materials. This effect is further exemplified by the results shown in figure 12, which shows the BFO dose-depth functions for the GCR spectra at solar minimum conditions. In addition to water and aluminum, results for liquid hydrogen (which may be used in application to propellant tank structures) show the dramatic superiority of this material as a shield. This is due largely to the greatly reduced generation of reaction products (nucleons and fragments) created by the GCR heavy ions traversing the hydrogen medium. For the very energetic GCR spectrum, most of the reduction in dose for all the materials shown occurs in the first 20–30 g/cm^2, with the magnitude of the dose gradient decreasing at larger thicknesses.

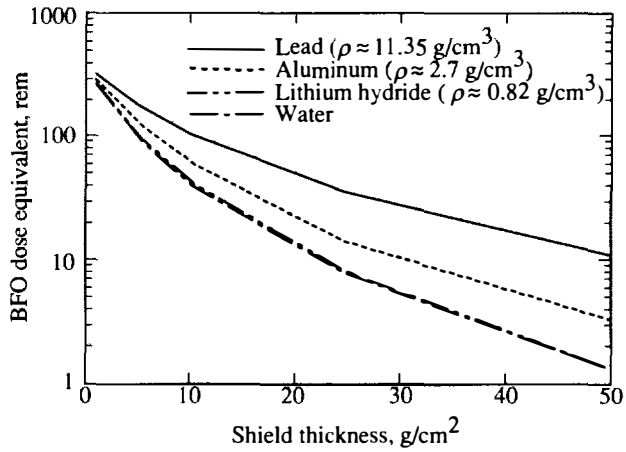

Figure 11. BFO dose equivalent versus depth functions for sum of 1989 flare fluences for four materials.

The differences between the GCR at solar minimum and maximum with respect to water shield thicknesses are shown in figure 13 (Townsend et al. 1990a). The incurred dose equivalents between these two extremes are seen to differ by about a factor of 2 for shield amounts up to 30 g/cm^2. These results were computed for the GCR spectra at solar minimum and maximum conditions as specified by the NRL CREME model. However, recent measurements (Kovalev et al. 1989) made during the last solar cycle imply that the GCR intensity during solar maximum may actually be greater than that prescribed in the NRL model.

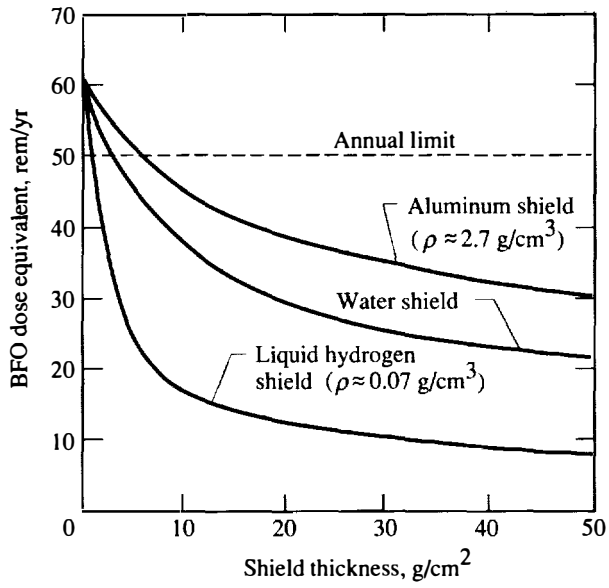

Figure 12. BFO dose equivalent as a function of shield type and thickness resulting from galactic cosmic rays at solar minimum conditions (Townsend et al. 1990a).

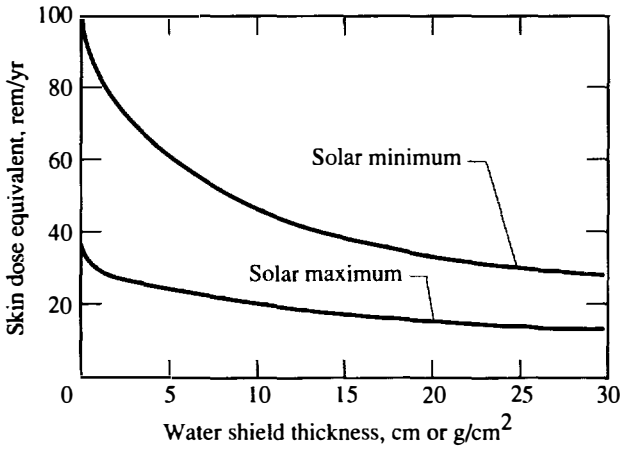

Figure 13. Dose equivalent as a function of water shield thickness resulting from galactic cosmic rays at solar minimum conditions (Townsend et al. 1990a).

The preceding paragraphs have dealt with the transport results for some of the more common materials that may be fabricated and/or supplied as shield media. For the surface habitats on the Moon and Mars, the regolith (or soil) of a particular locale is a convenient candidate for bulk shielding. In the analyses presented herein, the regolith composition is modeled using the mass-normalized concentrations of the five most abundant elements found in the soil. The lunar model composition is based on Apollo return samples (Dalton and Hohmann 1972), and the Martian model composition is based on Viking Lander data (Smith and West 1983). The normalized compositions used in the regolith shielding studies are given in table 2 (Nealy et al. 1988; Simonsen et al. 1990b). Moderate changes in composition are found to have negligible effects on the overall shielding properties (Nealy et al. 1988, 1989). As might be expected from the similarity of the Mars and lunar constituents, the regolith shielding characteristics are comparable.

The results of BFO dose versus depth in lunar regolith are given for the three large flares of solar cycles XIX and XX in figure 14. The regolith results are very similar to those for aluminum (fig. 10), which is not surprising since the mean molecular weight of the lunar regolith is comparable with the atomic weight of aluminum. Figure 15 shows the calculated propagation data for the GCR at solar minimum

Table 2. Composition of Lunar and Martian Regolith

Property	Lunar regolith	Martian regolith
Composition, normalized mass percentage	52.6 percent SiO_2 19.8 percent FeO 17.5 percent Al_2O_3 10.0 percent MgO	58.2 percent SiO_2 23.7 percent Fe_2O_3 10.8 percent MgO 7.3 percent CaO
Density, g/cm^3	0.8–2.15	1.0–1.8

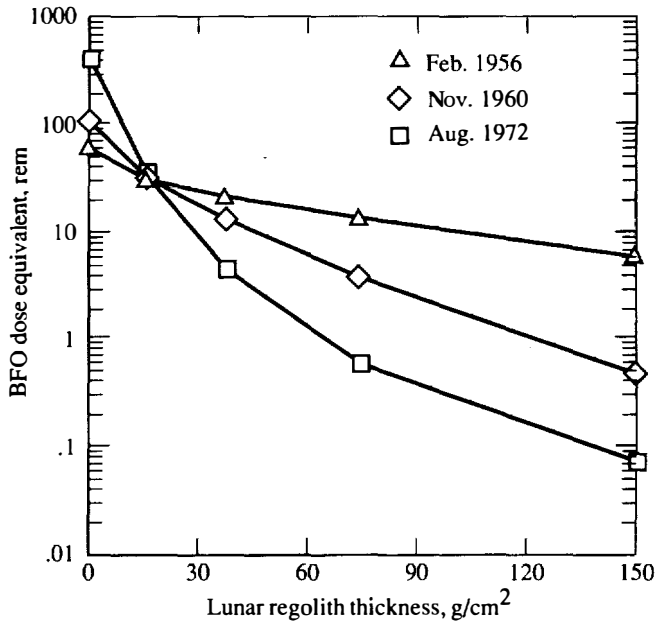

Figure 14. Predicted BFO dose equivalent for slab thickness between 0 and 150 g/cm^2 in simulated lunar regolith for flare events of August 1972, November 1960, and February 1956 (Nealy et al. 1988).

conditions, with the contributions to the dose by neutrons, protons, alphas, and two groups of heavier ions shown individually. For very thin layers, the heaviest ion group ($10 \leq Z \leq 28$) contributes over half the dose. For increasing thicknesses, the heavier ions fragment and react with target nuclei to produce particles of lower mass (ultimately, nucleons), which then deliver the greater percentage of the dose. For the lunar soil, approximately 90 percent of the dose is estimated to result from nucleons (mostly secondaries) for shield layers greater than approximately 20 g/cm^2.

The case of exposures on Mars differs considerably from the lunar situation because of the carbon dioxide atmosphere on Mars. Consequently, dose-depth functions are generated in carbon dioxide for the flare spectra of figure 3, and these results are shown in figure 16. The shielding effectiveness per unit mass of carbon dioxide is greater than the effectiveness of either aluminum or regolith results as shown previously (figs. 10 and 14, respectively). This is particularly the case for shield amounts exceeding 25 to 30 g/cm^2 of material. A similar observation may be made for the GCR results for carbon dioxide (fig. 17) compared with the corresponding calculations for aluminum and lunar regolith (figs. 12 and 15, respectively). The basic carbon dioxide propagation data may be applied to the Martian atmosphere when gas density as a function of altitude is specified.

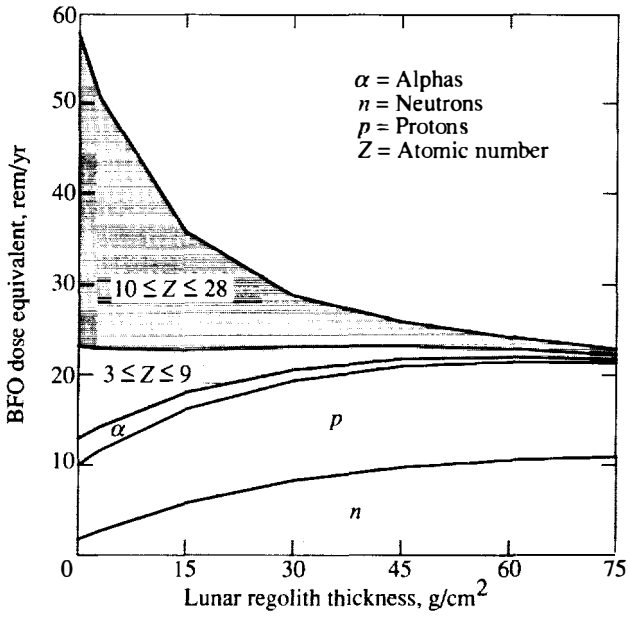

Figure 15. BFO annual dose-equivalent contributions from specified particle constituents as a function of lunar regolith thickness for GCR at solar minimum conditions (Nealy et al. 1989).

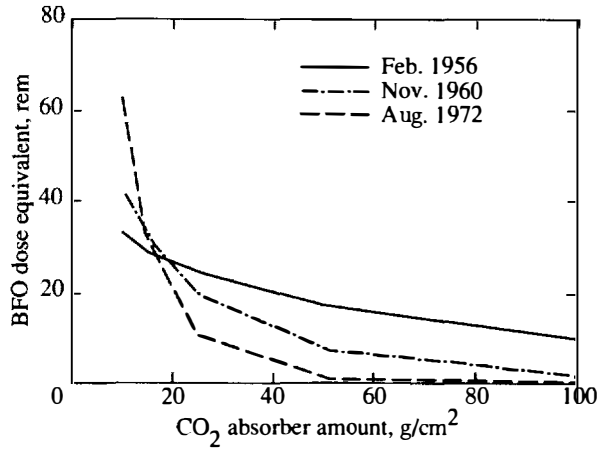

Figure 16. BFO dose equivalent as a function of carbon dioxide absorber amount for three solar flare events (Simonsen et al. 1990a).

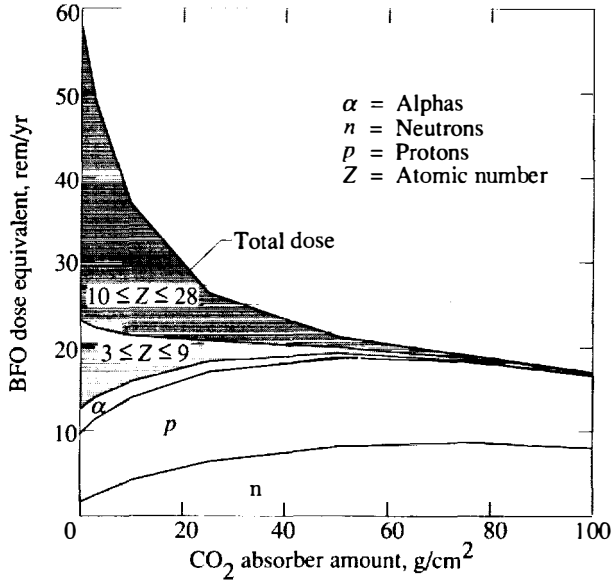

Figure 17. Annual BFO dose-equivalent contributions from specified particle constituents as a function of carbon dioxide absorber amount for GCR at solar minimum conditions (Simonsen et al. 1990a).

When Martian regolith is considered as a protective shield medium, the transport calculations must be made for the atmosphere-regolith thicknesses combined. In this case, the detailed flux/energy spectra emergent from a specified carbon dioxide amount must be used as input for the subsequent regolith calculation. Sample BFO dose results for such a procedure are given in figure 18 where fixed carbon dioxide amounts are used in conjunction with regolith layers. Two GCR cases and the energetic 1956 solar flare are included in the analysis. For moderate carbon

dioxide absorber amounts, the dose reductions from additional regolith layers are small compared with the dose reduction occurring in the first few g/cm^2 of carbon dioxide (figs. 16 and 17).

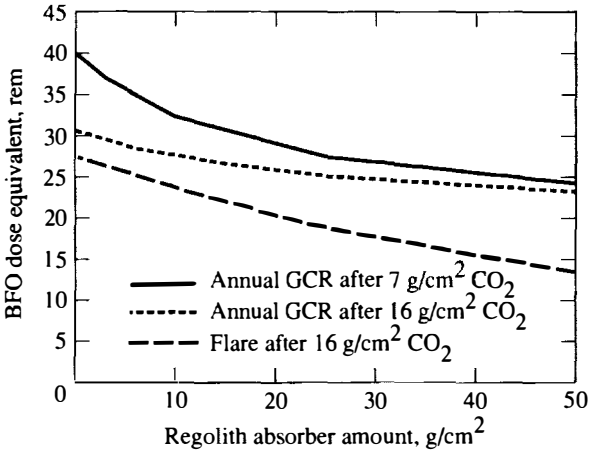

Figure 18. BFO dose equivalent as a function of regolith absorber amount after transport through Martian atmosphere in vertical direction (Simonsen et al. 1990b).

Description of Shield Assessment Results

When the computed propagation data for the GCR and solar flare protons in different materials are applied to specific shield geometries, the dose at a specific target point can be evaluated. To evaluate the dose at a particular point, the radiation from all directions must be determined. In free space, radiation will surround the crew from the full 4π steradians. However, on a planetary surface, only a solid angle of 2π is considered because the mass of the planet protects the crew from half of the free-space radiation. The dose contribution attributed to particles arriving from a given direction is determined by the shield thickness encountered along its straight-line path to a specified target point. For shield assessments in these analyses, the absorber amounts and the corresponding dosimetric quantities are evaluated for zenith angles between 0° and 90° in 5° increments and for azimuth angles between 0° and 360° also in 5° increments. The directional dose is then numerically integrated over the solid angle (4π for free space, 2π for planetary applications) about a target point to determine the total dose at that point. For free-space calculations in the case where a spherical shielded volume is considered, the slab- dose calculations can be used directly (fig. 9). Dose estimates using the propagation data for various materials are determined for the following shielded volumes: interplanetary transportation vehicles, lunar habitats, and Martian habitats.

Transportation Vehicles

Unshielded BFO dose equivalents in free space are substantial, and they could be lethal if an unusually large flare occurred. From galactic cosmic radiation at solar minimum conditions, an unshielded astronaut would receive approximately 60 rem/yr. The three large flare events of August 1972, November 1960, and February 1956 would have delivered unshielded BFO doses of approximately 411 rem, 110 rem, and 62 rem, respectively. The GCR dose is over the annual BFO limit of 50 rem/yr and the flare doses are significantly greater than the 30-day limit of 25 rem. Clearly, both lunar and Mars transportation vehicles must offer adequate protection. The protection for the short lunar travel time will most likely emphasize flare protection, whereas the protection for the longer travel time to Mars must consider both the GCR and the flares combined. The following analyses consider radiation protection for transportation vehicles required for various flare scenarios and for galactic cosmic radiation.

Solar flare analysis. The normal incident slab calculations presented in the previous section can be used to estimate the doses inside nearly spherical structures in an assumed isotropic radiation field. Results of such an application are presented in table 3 for the three large solar flare events (Townsend et al. 1989). The aluminum shield thicknesses required to reduce the incurred dose from large flares to the astronaut 30-day limit for the eye, skin, and blood-forming organs are estimated. Even though the individual flare spectra exhibit marked differences (fig. 3), the required shield thickness ranges from approximately 18 to 24 g/cm^2 (7 to 9 cm) of aluminum. The shield mass required can be reduced by approximately 15 to 30 percent using water as shielding with thicknesses of only 15 to 20 g/cm^2 required (Townsend et al. 1989). These shielding estimates include only a flare contribution and represent a minimum acceptable wall thickness. Rather than shielding an entire spacecraft with these wall thicknesses, the crew can be provided with a heavily shielded "shelter" for protection during a large flare event.

Solar cycle XXI analysis. For long-duration missions, contributions from the GCR and the more numerous smaller flares should be considered. Dose evaluations throughout a complete solar cycle are made using the flare data (fig. 4) measured during solar cycle XXI between 1975 and 1986 (Nealy et al. 1990). The GCR contribution is assumed to vary

sinusoidally from peak values at solar minimum to the smallest dose rate at solar maximum. Normal incident slab calculations for the dose evaluations are made using effective water shield thicknesses. Water, both potable and waste, may be a likely shield material for long-duration missions since it will probably be available in large quantities. Water calculations can be used to simulate results for other media of low atomic weight and high hydrogen content. Consequently, reasonable shield mass requirements may be estimated on the basis of water transport results.

Table 3. Aluminum Shield Thickness Required for Solar Flare Protection To Remain Below the 30-Day Limit

[Data from Townsend et al. 1989]

Organ	Aluminum shield thickness for solar flare event—					
	February 1956		November 1960		August 1972	
	g/cm^2	cm	g/cm^2	cm	g/cm^2	cm
Skin . . .	1.3	0.5	2.5	1.0	7.5	2.8
Eye	1.5	0.6	3.5	1.3	9.5	3.5
BFO . . .	24.0	8.9	22.0	8.1	18.0	6.7

Figures 19 and 20 show sample BFO dose estimates from this study as a function of time within the solar cycle. In figure 19, the dose equivalent incurred for an effective water shield of 5 g/cm^2 is given for mission durations of 3, 12, and 36 months. The figure shows the dose integrated over the mission duration time, with the flare contribution (according to the solar cycle XXI distribution) appearing as deviations above the smooth sinusoidal curve, which would be seen for the GCR contribution alone. The results indicate that the flare contribution is not conspicuous in comparison to the more regularly varying GCR component. For missions of duration longer than 1 year, one may conclude that the dose contributions due to the normally occurring solar flares are not significant in comparison with the GCR (for shield amounts greater than 5 g/cm^2). In this case, the cumulative dose is approximately proportional to the mission duration time.

The BFO dose received by crew members on a 3-, 12-, or 36-month mission starting in any portion of the solar cycle may be predicted from figure 19. For example, the final dose value on figure 19(c) of about 125 rem represents the dose incurred for a mission beginning 8 years after solar minimum and lasting over the next 3 years. This plot (fig. 19(c)) also indicates that a 3-year mission beginning 4 years after solar minimum would result in a total incurred dose approximately 45 percent lower than would be received on a mission beginning at solar minimum.

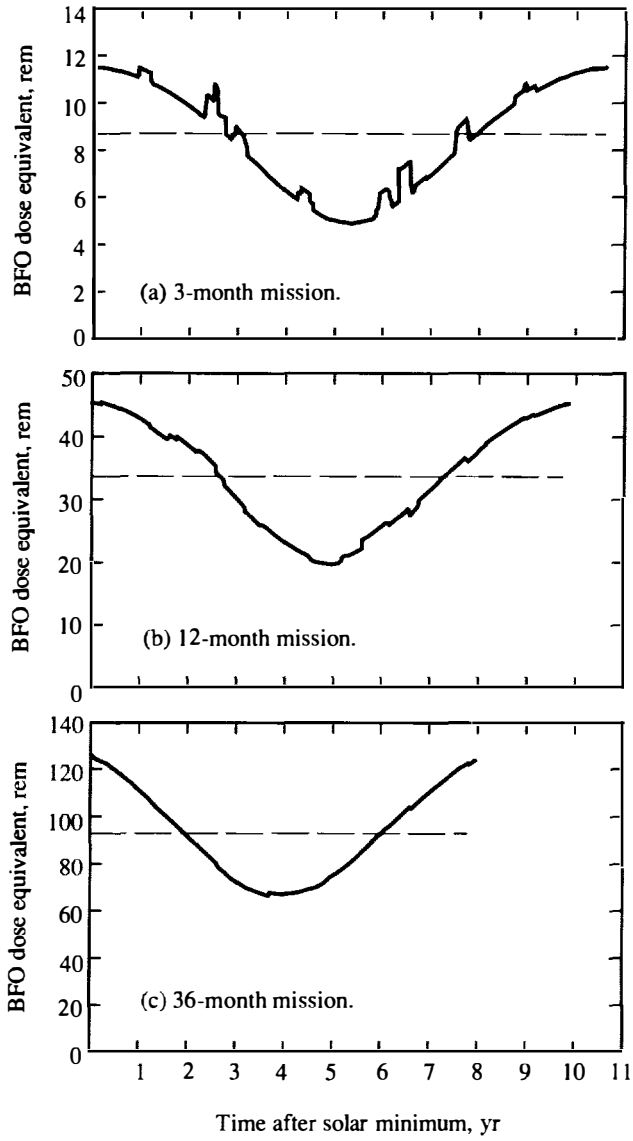

Figure 19. Free-space BFO dose equivalent incurred for 5-g/cm^2-thick water slab shields for three mission lengths as a function of time in cycle after solar minimum conditions. Dashed lines indicate the average cycle value (Nealy et al. 1990).

Figure 20 illustrates the variation of the cumulative incurred dose equivalent throughout an entire solar cycle for 5- and 15-g/cm^2 water shield amounts. This type of representation is useful in estimating the incurred dose for long-duration missions (2 years or more) that begin and end at arbitrary times within the solar cycle. For example, from figure 20(a), the total BFO dose for a 5-year mission beginning at solar minimum is predicted to be approximately

180 rem for 5-g/cm^2 shielding. However, if the 5-year mission begins 3 years after solar minimum, the total incurred dose is estimated to be approximately 135 rem (260 rem at year 8 minus 125 rem at year 3).

The preceding results from the solar cycle XXI analysis do not include contributions from a rarely occurring giant solar proton event (e.g., the events of 1956, 1960, 1972, and 1989), and such an event must be accounted for separately as circumstances warrant. For example, for a 1- or 2-year mission spanning the solar minimum conditions, a large proton event would be highly unlikely, whereas during active Sun conditions, a larger (but still relatively small) probability exists that incurred doses would be considerably increased because of large flare episodes.

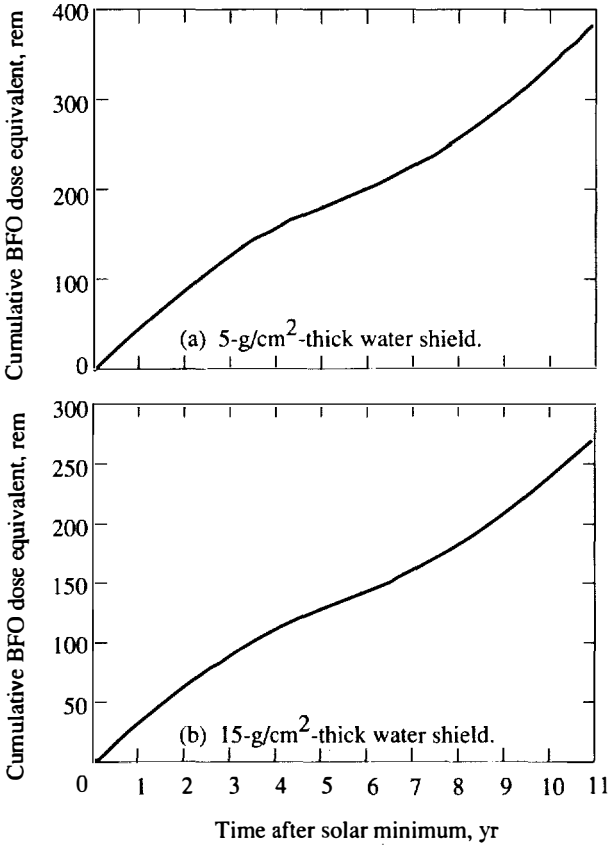

Figure 20. Cumulative total BFO dose-equivalent variation incurred throughout 11-year solar cycle for water slab shields (Nealy et al. 1990).

Shield mass estimates. The results of the solar cycle XXI study indicate that a reasonably conservative radiation environment for exposure analysis may be derived from the solar minimum GCR flux with the inclusion of one large proton event. The BFO dose-depth variation for such an environment consisting of the fluence of the 1972 large proton event in combination with the annual GCR contribution is given in figure 21. The 50-rem BFO dose-equivalent value is exceeded for water shield amounts less than about 18 g/cm^2. For shields thicker than 25 or 30 g/cm^2, the flare dose is insignificant. This propagation data can be used to estimate shield masses of various manned habitation modules.

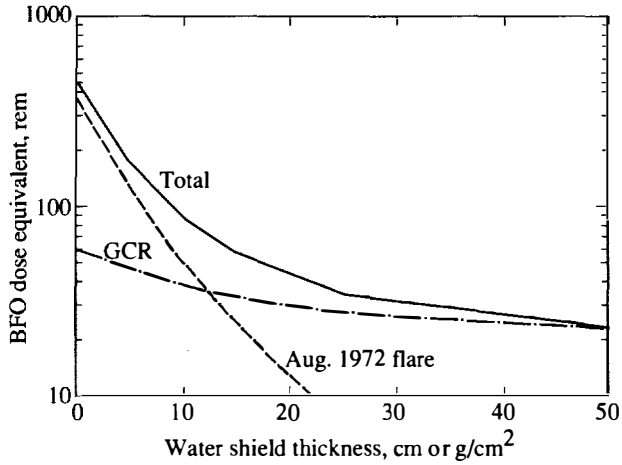

Figure 21. BFO dose-depth equivalent as a function of water shield thickness for August 1972 flare and the GCR at solar minimum conditions.

Guidelines for manned-module volume requirements are graphically depicted in figure 22 (NASA STD-3000, 1987). According to these guidelines, long-duration missions would require at least 10 m^3 per crew member as a performance limit and approximately 19 m^3 as an optimal limit. (Here, the tolerance limit volume is not considered to be applicable for normal operations on extended missions.) A four-person crew is recommended for a manned Mars mission (The 90-Day Study), which implies a

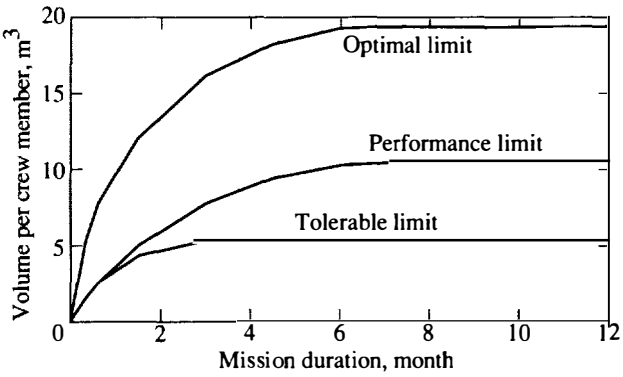

Figure 22. Guidelines for determination of total habitable volume required per person in a space module (NASA STD-3000, 1987).

minimum habitable volume of approximately 42 m^3. If a cylindrical module is assumed, with diameter equal to length, the shield mass of the configuration may then be found as a function of dose delivered near the center of the module. Figure 23 shows the annual delivered dose due to GCR and the August 1972 flare as a function of cylinder shield mass. Again, equivalent water shield thicknesses are used in these estimates (fig. 21). If one considers an acceptable design criterion to be 50 to 70 percent of the maximum allowable dose, then shield masses on the order of 20 to 30 metric tons are required for the 42-m^3 volume. Shield mass estimates will be greater if aluminum is assumed to be the shielding material because of the poorer shielding characteristics of aluminum. In some cases, the shield mass can be a significant fraction of the total mass of candidate Mars transportation vehicle concepts (The 90-Day Study). However, the bulk shield mass is not necessarily the extra mass that must be provided, but the total shielding required which can include the pressure vessel walls, water tanks, fuel tanks, and other components of the spacecraft.

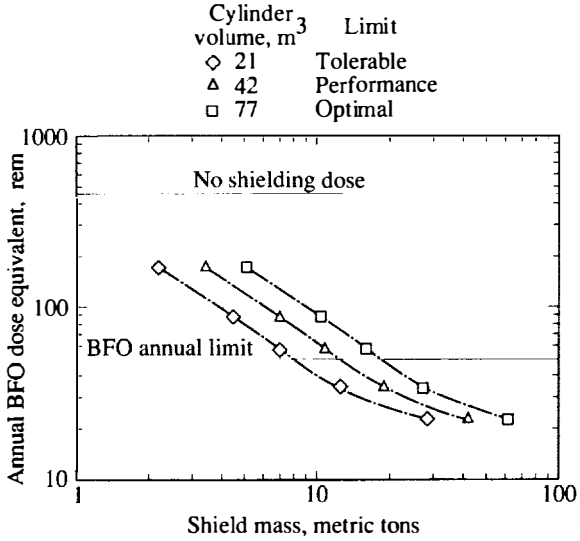

Figure 23. BFO dose equivalent incurred from the August 1972 flare and the GCR (fig. 21) versus shield mass for cylindrical modules (Length/Diameter = 1.0) of various volumes based on requirements of figure 22 for four-man crew.

Analysis of a Mars transfer-vehicle concept. The basic propagation data generated in the form of slab dose estimates can also be used for more detailed dose analyses of specific shielded configurations. One such configuration, depicted in figure 24, is a manned Mars transfer-vehicle concept developed by Martin Marietta. This concept contains two cylindrical habitat modules (diameter of 7.6 m, length of 2.7 m). For the sample calculations, the combination of components and bulk shielding for each habitat module is assumed to be equivalent to an effective water shield thickness of 5 g/cm^2. Also, contributing to the shielding for the dose calculations are the ECCV, pantry, and fuel tanks.

The directional dose due to GCR (at solar minimum) was calculated for an interior point in the center one of the habitat modules. Figure 24 shows the axisymmetric directional dose pattern superimposed on the vehicle configuration outline. This pattern consists of vectors emanating from a target point with their lengths proportional to the annual GCR dose per unit solid angle. Although the radiation field outside the spacecraft is assumed to be isotropic, geometry effects cause the internal field to be highly anisotropic. In particular, very little radiation penetrates from solid angles subtending the fuel tanks, which in the illustrative calculation are assumed to be full. By numerically integrating the directional dose, the BFO dose in the center of Hab A is estimated to be 29 rem/yr.

Total BFO dose estimates are also predicted for a variety of points within each module from which contours of the dose variation are obtained. Figure 25 shows the BFO dose variation within the habitat modules. The influence of the fuel tanks is evident in the lower overall doses of the module closest to the fuel supply (Hab A). The large dose gradient evident at the top of Hab B is due to the thick walls of the adjacent pantry or flare shelter. Analyses such as these are expected to be of importance in the design stages of free-space modules with regard to crew-quarters layouts, placement of equipment, storage of consumables and waste, etc.

Lunar Surface Habitation

Once on the surface of the Moon, the radiation hazards of free space will be less severe. Unshielded BFO dose estimates for the flare events of August 1972, November 1960, and February 1956 are approximately half of those of free space: 205 rem, 55 rem, and 31 rem, respectively. These dose estimates are significantly higher than the 30-day limit of 25 rem. The BFO dose incurred from the GCR at solar minimum is estimated to be approximately 30 rem/yr, which is below the 50-rem/yr annual limit. However, the GCR dose in conjunction with medium to large flare-event doses may reach the annual limit and become career limiting for long-duration missions. These values clearly show the need for radiation protection while on the lunar surface. Local resources, such as lunar regolith, will be available for use as protective shielding to cover

habitats. In this section, several habitat configurations are considered with different regolith shield thicknesses for protection.

Dose calculations inside candidate habitats are predicted using the computed propagation data for solar flares and the GCR shown in figures 14 and 15. A conservative estimate of the free-space environment is to assume the combination of the GCR at solar minimum and one large proton event. From figures 14 and 15, the regolith slab dose estimates imply that a 50-cm thickness (75 g/cm^2 assuming a regolith density of 1.5 g/cm^3) will reduce the BFO dose equivalent to approximately 40 rem for the sum of the GCR and one large flare (February 1956). With the 2π steradian shielding on the lunar surface, it is expected that with a 50-cm regolith layer, the annual dose for this environment is reduced to approximately 20 rem. Thus, a 50-cm shield thickness is selected for analysis to reduce dose levels to slightly less than half of the annual limit (or a design safety factor of approximately 2). Shield thicknesses of 75 and 100 cm are also selected for analysis to determine the extent to which additional shielding will further reduce annual doses.

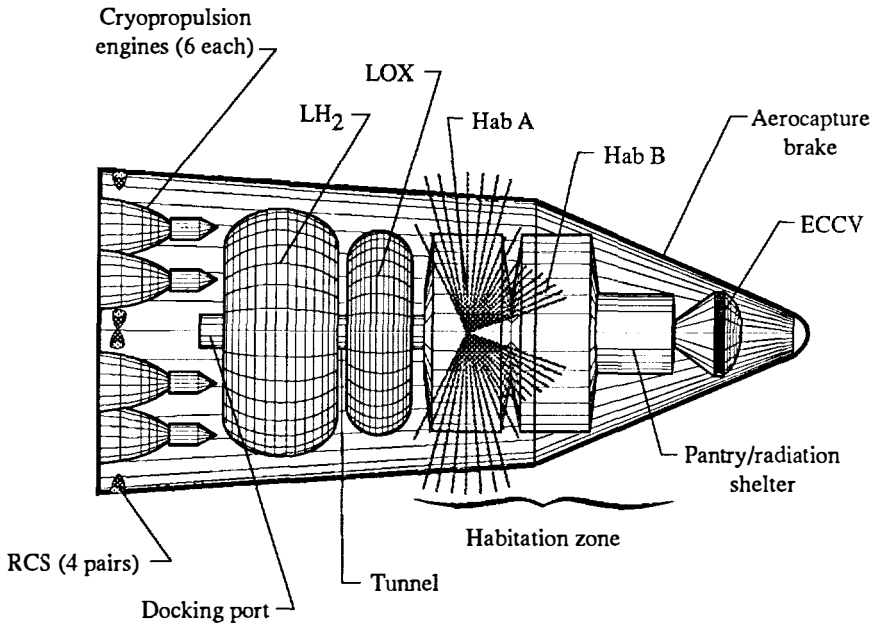

Figure 24. Configuration of Martian piloted vehicle with sample directional dose patterns for a point inside Hab A module.

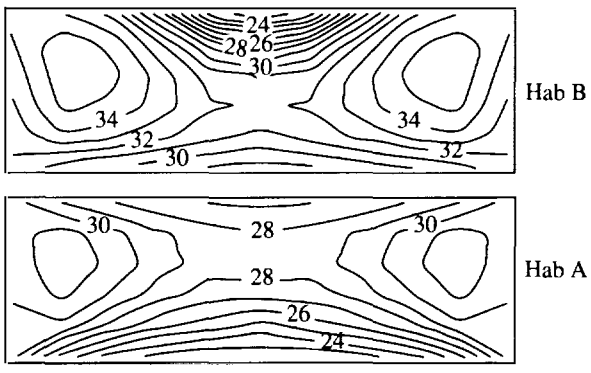

Figure 25. Annual BFO dose-equivalent variation due to galactic cosmic radiation for the cylindrical habitat modules shown in the conceptual Mars vehicle configuration. Contour increments are 1 rem/yr.

Early lunar habitats are described as a Space Station *Freedom* derived module and an inflatable/constructible sphere (Alred et al. 1988). The Space Station derived module is assumed to be 4.6 m in diameter and 12.2 m in length as shown in figure 26(a). The module is assumed to be lengthwise on the lunar surface and covered with either 50 cm (or 75 g/cm^2 assuming a regolith density of 1.5 g/cm^3) or 100 cm of lunar regolith overhead. Along the sides, the regolith material is filled in around the cylinder to form a vertical wall up to the central horizontal plane. For the 50-cm layer, the shield thickness will vary from 230 to 50 cm from ground level up to this plane. The spherical habitat is 15.2 m in diameter and is modeled as a half-buried sphere with the portion above ground level shielded with a 50-, 75-, or 100-cm regolith layer (fig. 26(b)).

The integrated BFO dose estimates that would have been incurred from the three solar flare events using shield thicknesses of 75 and 150 g/cm^2 are shown in table 4 (Nealy et al. 1988). The values in the table represent the dose in the center of the habitat for each flare event. The dose distribution was also calculated throughout each habitat. For the cylindrical module, the general dose levels show little change for heights above and below the center plane. The radiation field maxima occur at about two-thirds the distance between the center and end walls. For the spherical habitat, the field maximum occurs above the center point at positions closer to the top, whereas doses in the buried half are significantly reduced. The BFO dose variations within these habitats for the November 1960 flare event are shown in figures 27 and 28.

Table 4. BFO Dose Comparisons for Three Large Solar Flares for Lunar Habitats

[Data from Nealy et al. 1988]

Flare data	Regolith thickness, cm	Predicted dose, rem	
		Cylinder (center)	Sphere (center)
1956	50	7.48	7.04
	100	2.70	2.94
1960	50	1.60	1.90
	100	.16	.23
1972	50	0.25	0.30
	100	.03	.04

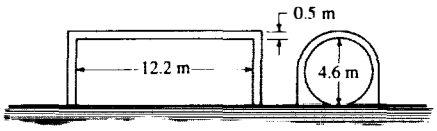

(a) Cylindrical module (side and end views).

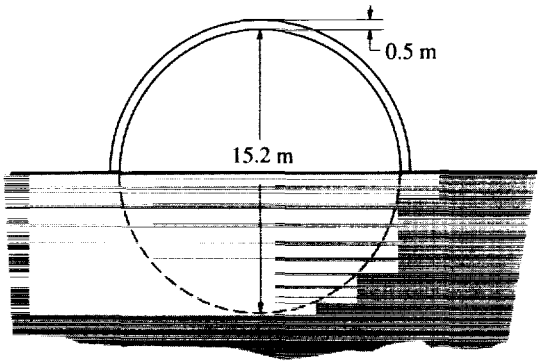

(b) Spherical module.

Figure 26. Modeled shielded configurations of candidate lunar habitat modules (Nealy et al. 1989).

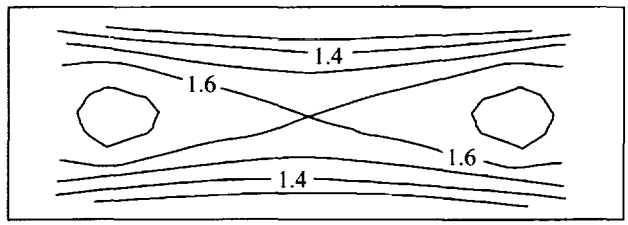

Figure 27. BFO dose-equivalent variation within a shielded cylinder for central horizontal plane resulting from November 1960 flare event. Dose values are in 0.1-rem contour increments for 75-g/cm^2-thick regolith shield overhead (Nealy et al. 1988).

Dose predictions are also included for the GCR at solar minimum conditions. The maximum integrated BFO doses estimated in each habitat for various shield thicknesses are shown in table 5 (Nealy et al. 1989). For the cylindrical habitat configuration, the dose variation throughout the configuration is relatively small (fig. 29). For the portion of the spherical habitat above ground level, the dose variation is also relatively small with a broad maximum dose rate observed directly above the sphere center point (approximately 11 to 12 rem/yr). Below ground level, a larger gradient in dose rate is shown in the downward direction, with values in the lower section decreasing to less than 5 rem/yr (fig. 30). With 112.5-g/cm^2-thick shielding overhead, the dose rate maximum is reduced to 8 to 10 rem/yr throughout the upper half of the sphere. This increased shielding is of even less significance in the regions below the ground where predicted doses approach the same low values as seen in the 75-g/cm^2 calculation. Relatively little reduction in dose (less than 20 percent) occurs for a 50-percent increase in layer thickness, indicating that further substantial dose reductions would require very thick layers of material.

Table 5. GCR Integrated BFO Results for Lunar Habitats

[Data from Nealy et al. 1989]

Habitat geometry	Regolith thickness		BFO dose equivalent, rem/yr
	cm	g/cm^2 (a)	
Cylindrical	50	75	12
Spherical	50	75	12
	75	112.5	10

[a]Assuming a regolith density of 1.5 g/cm^3.

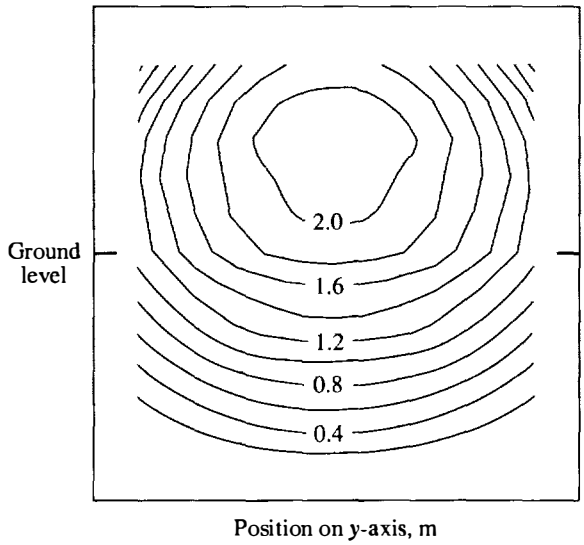

Figure 28. BFO dose-equivalent variation within half-buried sphere shielded overhead with 75-g/cm^2-thick regolith layer resulting from November 1960 flare event. Dose values are in 0.2-rem contour increments (Nealy et al. 1988).

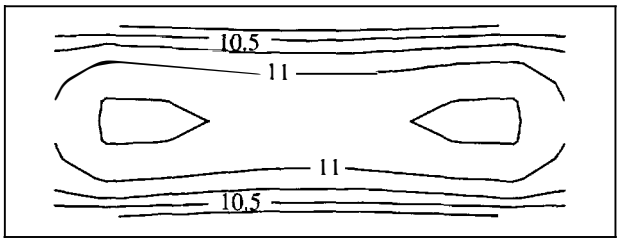

Figure 29. Annual BFO dose-equivalent variation within shielded cylinder for central horizontal plane resulting from GCR. Dose values are in 0.25-rem/yr contour increments for 75-g/cm^2-thick regolith shield overhead (Nealy et al. 1989).

A conservative yearly estimate of dose is to assume that the crew receives the dose delivered from the GCR and the dose delivered from one large flare (in this case, the February 1956 flare since it delivers the largest dose in the shielded module). If 75 g/cm^2 of regolith is selected for coverage, such a BFO dose in the cylindrical habitat is approximately 19.5 rem/yr. Estimating the dose in the spherical habitat is more complicated because of the large variation in dose throughout the habitat; however, the maximum dose estimated is approximately 19 rem/yr. These dose estimates are well below the 50-rem/yr established guidelines for United States astronauts. The 30-day limit, with regard to the flares, remains below the 25-rem limit. The skin doses, not presented in this analysis, are also well below the established 30-day and annual limits. The above estimates have not taken into account the added shielding provided by the pressure vessel wall, supporting structures, or the placement of equipment in and around the module.

Shielding from solar flare events is essential on the lunar surface whether in the form of heavily shielded areas (i.e., flare shelters) or overall habitat protection for any mission duration. For longer stay times on the surface, the shielding from GCR becomes necessary to reduce the crew member's overall career exposure. A regolith shield thickness of 50 cm is estimated to provide adequate flare and GCR protection. However, before an optimum thickness and shielding strategy are selected, the complete mission scenario (including the lunar transport vehicle) needs to be studied in detail.

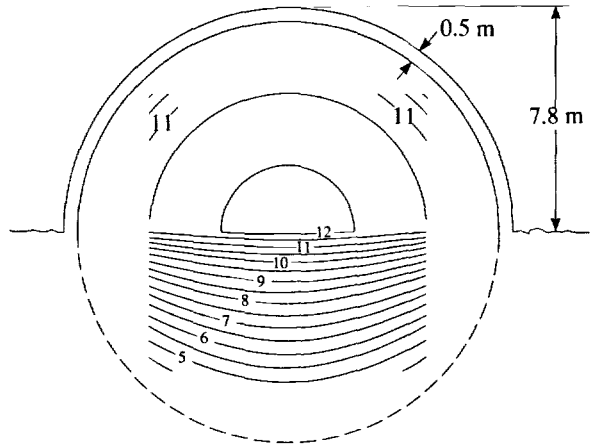

Figure 30. Annual BFO dose-equivalent variation within half-buried sphere shielded overhead with 75-g/cm^2-thick regolith layer resulting from GCR. Dose-equivalent values are in contour intervals of 0.5 rem/yr (Nealy et al. 1989).

Martian Surface Habitation

The radiation environment on the Martian surface is less severe than that found on the lunar surface. Although Mars is devoid of an intrinsic magnetic field strong enough to deflect charged particles, it does have a carbon dioxide atmosphere that will help protect surface crews from free-space radiative fluxes. Estimating the unshielded doses anticipated for crew members on the surface of Mars is more difficult than estimates made for the lunar surface in which free-space estimates are simply divided in half. Now, the protection provided by the atmosphere must be considered.

Atmospheric shielding analysis. The amount of protection provided by the Martian atmosphere depends on the composition and structure of the atmosphere and the crew member's altitude. In

this analysis the composition of the atmosphere is assumed to be 100 percent carbon dioxide. The Committee on Space Research has developed warm high- and cool low-density models of the atmospheric structure (Smith and West 1983). The low-density model and the high-density model assume surface pressures of 5.9 mb and 7.8 mb, respectively. The amount of protection provided by the atmosphere, in the vertical direction, at various altitudes is shown in table 6 (Simonsen et al. 1990a). In these calculations, a spherically concentric atmosphere is assumed such that the amount of protection provided increases with increasing zenith angle. Dose predictions at altitudes up to 12 km are included in the analysis because of the large topographical relief present on the Martian surface.

Table 6. Martian Atmospheric Protection in Vertical Direction

Altitude, km	Low-density model, g CO_2/cm^2	High-density model, g CO_2/cm^2
0	16	22
4	11	16
8	7	11
12	5	8

Dose estimates are predicted for the galactic cosmic radiation for the minimum of the solar activity cycle (fig. 6). The fluence spectra at 1 AU are used for the three large flares of August 1972, November 1960, and February 1956 (fig. 3). In the vicinity of Mars (approximately 1.5 AU), the fluence from these flares is expected to be less; however, there is still much discussion on the dependence of the radial dispersion of the flare with distance. Therefore, for the flare calculations in this analysis, the free-space fluence-energy spectra at 1 AU have been conservatively applied to Mars. The surface doses at various altitudes in the atmosphere are determined from the computed propagation data for the GCR and the solar flare protons through carbon dioxide as shown in figures 16 and 17.

Integrated dose-equivalent calculations were made for both the high- and low-density atmospheric models at altitudes of 0, 4, 8, and 12 km. The corresponding skin and BFO dose estimates are shown in tables 7 and 8, respectively (Simonsen et al. 1990a). A total yearly skin and BFO dose may be conservatively estimated as the sum of the annual GCR dose and the dose from one large flare. At the surface, such an estimated skin dose equivalent is 21 to 24 rem/yr and an estimated BFO dose equivalent is 19 to 22 rem/yr (GCR plus 1956 event). At an altitude of 12 km, an estimated skin dose equivalent is 61 to 105 rem/yr and an estimated BFO dose equivalent is 33 to 48 rem/yr (GCR plus 1972 event). These dose predictions imply that the atmosphere of Mars may provide shielding sufficient to maintain the annual skin and BFO dose levels below the current 300 rem/yr and the 50 rem/yr United States astronaut limits, respectively.

Table 7. Integrated Skin Dose Equivalents for Martian Atmospheric Models

[Data from Simonsen et al. 1990a]

		Integrated skin dose equivalent, rem, at altitude of—			
		0 km	4 km	8 km	12 km
Galactic cosmic ray (annual)	High density	11.3	13.4	15.8	18.6
	Low density	13.2	15.9	18.9	22.4
Aug. 1972 solar flare event	High density	3.9	9.5	21.1	42.8
	Low density	9.0	21.9	46.2	82.6
Nov. 1960 solar flare event	High density	6.4	10.0	14.8	21.1
	Low density	9.7	15.1	21.9	29.6
Feb. 1956 solar flare event	High density	9.2	11.1	13.3	15.9
	Low density	11.0	13.4	16.2	19.1

The 30-day limits are important when considering the doses incurred from a solar flare event. The only 30-day limit exceeded is the BFO limit of 25 rem for the August 1972 event at the altitude of 12 km. However, as seen in figure 16, the August 1972 flare is rapidly attenuated by matter, and a few g/cm^2 of additional shielding should reduce the anticipated dose below this limit. These dose predictions imply that the atmosphere of Mars may also provide sufficient shielding to maintain 30-day dose levels for the skin and BFO below the current 150-rem and 25-rem astronaut limits, respectively.

Regolith shielding analysis. Mars exploration crews are likely to incur a substantial dose while in transit to Mars and perhaps from other radiation sources (e.g., nuclear reactors) which will reduce the allowable dose that can be received while on the surface. Therefore, additional shielding may be necessary to maintain short-term dose levels below limits or to help maintain career dose levels as low as possible. By utilizing local resources, such as

Martian regolith, shielding materials can be provided without excessive launch weight requirements from Earth.

Table 8. Integrated BFO Dose Equivalents for Martian Atmospheric Models

[Data from Simonsen et al. 1990a]

		Integrated BFO dose equivalent, rem, at altitude of—			
		0 km	4 km	8 km	12 km
Galactic cosmic ray (annual)	High density	10.5	12.0	13.7	15.6
	Low density	11.9	13.8	15.8	18.0
Aug. 1972 solar flare event	High density	2.2	4.8	9.5	17.4
	Low density	4.6	9.9	18.5	30.3
Nov. 1960 solar flare event	High density	5.0	7.5	10.6	14.4
	Low density	7.3	10.8	14.8	19.1
Feb. 1956 solar flare event	High density	8.5	10.0	11.7	13.4
	Low density	9.9	11.8	13.6	15.3

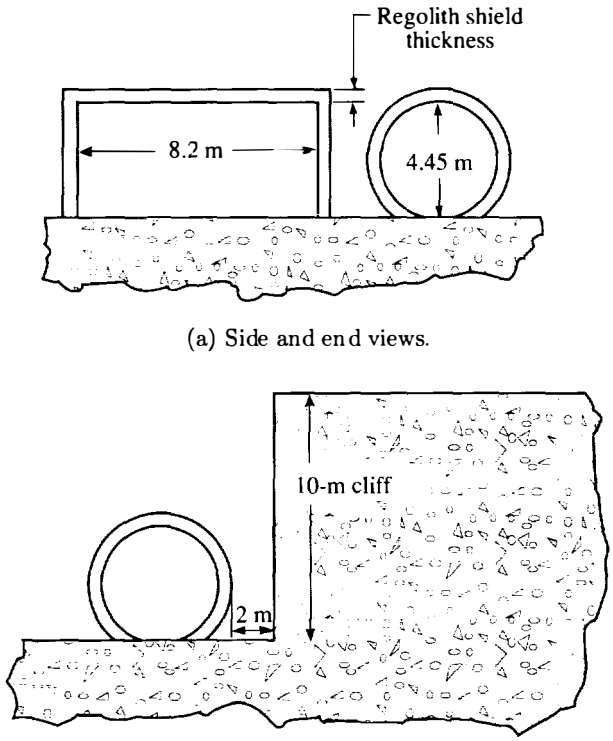

(a) Side and end views.

(b) End view of module next to cliff.

Figure 31. Cylindrical habitat module with regolith shielding for Mars (Simonsen et al. 1990b).

The GCR particle flux and solar flare particle flux spectra obtained during the atmosphere calculations at 0- and 8-km altitudes are now used as input conditions for regolith shield calculations. For a representative large solar flare contribution, the very penetrating spectrum of the February 1956 event is selected for further analysis. This event has the greatest flux of high-energy particles which results in the highest dose at the Martian surface. The subsequently calculated particle flux versus energy distributions in the regolith can then be used to determine the dose at specified locations in the shield media. The dose contribution attributed to particles arriving from a given direction is now determined by the amount of CO_2 traversed and then the shield thickness encountered along its straight-line path to a specified target point. An example of some of the basic propagation data required is shown in figure 18.

One early Martian habitat is described as a Space Station *Freedom* derived module that is 8.2 m in length and 4.45 m in diameter (The 90-Day Study). The cylindrical module is assumed to be lengthwise on the Martian surface with various thicknesses of Martian regolith surrounding it. Another configuration assumes that the module is situated 2 m from a 10-m-high cliff. (See fig. 31.)

A series of calculations are performed for various regolith thicknesses covering the module. Again, no consideration is given to the added shielding provided by the pressure vessel and internal equipment. The largest integrated dose equivalent in a vertical plane through the center of the cylinder is plotted versus an effective regolith shield thickness in figure 32 (Simonsen et al. 1990b). As shown in the figure, the regolith does not provide much additional protection from the GCR or the flare event than that already provided by the carbon dioxide atmosphere. The slope of each curve is relatively flat after 20 g/cm^2, with most of the skin and BFO dose reductions occurring in the first 20 g/cm^2. For 20 g/cm^2 of regolith protection, the annual BFO dose equivalent due to the GCR is reduced from 11.9 to 10.0 rem/yr at 0 km, and from 15.8 to 11.2 rem/yr at 8 km. The annual skin dose equivalent is reduced from 13.2 to 11.0 rem/yr at 0 km, and from 18.9 to 12.6 rem/yr at 8 km. For 20 g/cm^2 of regolith protection, the BFO dose equivalent due to the solar flare is reduced from 9.9 to 6.3 rem/event at 0 km. The skin dose equivalent is reduced from 11.0 to 6.9 rem/event.

For the GCR, the dose variation within the module in the radial direction is not large, approximately 5 to 20 percent for 15 to 50 cm of shielding, respectively. For the February 1956 solar flare event, the dose-equivalent variation is between approximately

25 to 40 percent for 15 to 50 cm of shielding, respectively. In the axial direction, the dose estimates for both the GCR and the flare showed a variation of less than 1 percent, which suggests that the doses incurred in cylindrical habitats of other lengths would be comparable in magnitude.

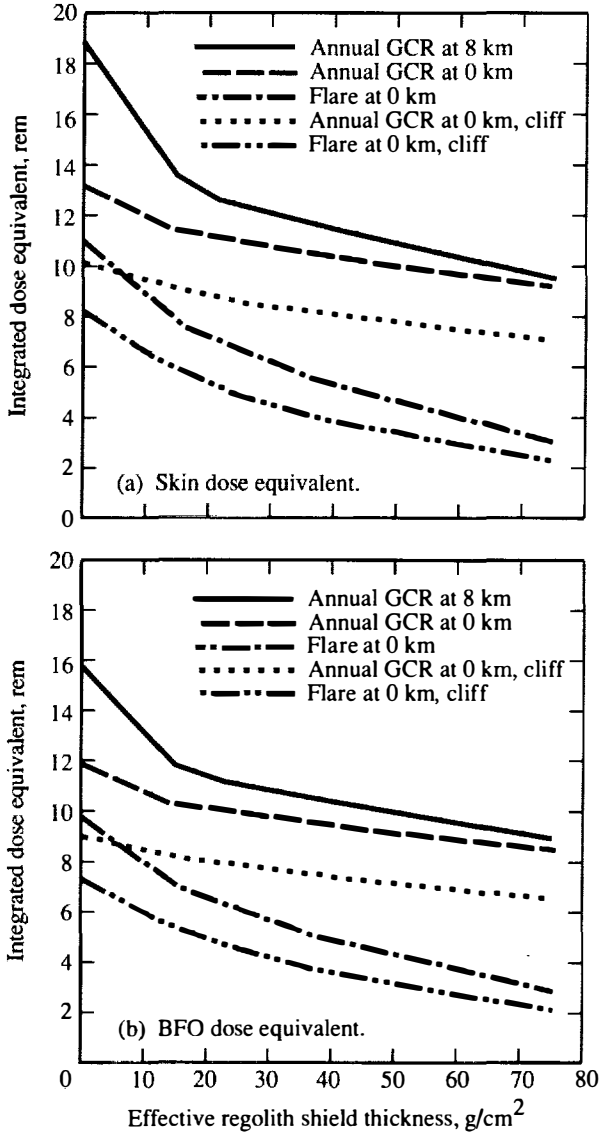

Figure 32. Maximum dose equivalent in central cross-sectional plane of module as a function of effective regolith shield thickness (Simonsen et al. 1990b).

A possible way to further reduce the dose equivalent received on the Martian surface would be to locate the habitat next to a cliff. As shown in figure 32(b), the cliff further reduces the BFO dose equivalent by approximately 2 to 3 rem/yr at 0 km for the GCR, and by approximately 1 to 1.5 rem/event at 0 km for the February 1956 flare. Similar decreases are also obtained for the skin dose equivalent (fig. 32(a)). The shielding provided by the cliff and atmosphere alone results in a BFO dose equivalent of 9.1 rem/yr for the GCR and of 7.4 rem/event for the February 1956 event.

From this analysis, it is concluded that moderate thicknesses of Martian regolith do not provide substantial additional protection to that already provided by the carbon dioxide atmosphere. If regolith is used as shielding material, the largest reduction in dose equivalent occurs in the first 20 g/cm^2 (or approximately 15 cm if assuming a regolith density of 1.5 g/cm^3). Thus, if additional protection using Martian regolith is desired, a shield thickness on the order of 15 to 20 cm is recommended. If additional protection using 15 cm of Martian regolith is provided at an altitude of 0 km, the annual skin and blood-forming organ dose equivalent will be reduced from 24 to 18 rem/yr and from 22 to 16 rem/yr, respectively (Simonsen et al. 1990b).

For radiation protection provided by regolith on the surface of Mars, mission planners and medical personnel must decide if the radiation doses anticipated warrant the added equipment and time required for crew members to "bury" themselves. For the shorter stay times of 30 to 90 days, the additional requirements placed on a Mars mission to cover a module may be unnecessary, especially if a flare shelter is provided. A logical alternative to massive shielding efforts is to take advantage of local terrain features found on the surface of Mars. Regolith shielding may become more attractive for the longer stay times of 600 days or for futuristic permanent habitation.

Issues and Concerns

Estimates and predictions of radiation exposure and incurred doses for space exploration missions usually require complex analysis techniques and involve uncertainties that are presently difficult to quantify. Some issues and concerns regarding radiation exposure estimates and shielding requirements are discussed in the following paragraphs.

Environment

Confidence in the estimates of incurred dose for lunar and Mars missions is directly related to the accuracy and development of the current space-radiation environmental models. With regard to the charged-particle environmental models, only in some cases do enough data exist for estimates of uncertainties and natural variabilities. At the present time, no particular flare model has been established as a practical standard. However, a likely future candidate is the statistical model developed at the Jet Propulsion

Laboratory (Feynman and Gabriel 1990). The continued development, endorsement, and implementation of standard environmental models is an important aspect of mission scenario analyses and shield design studies.

Transport Codes

The accuracy of transport codes used to describe the propagation of particles through matter is another concern. Monte Carlo techniques are generally regarded as most faithfully representing the details of the complex processes involving high-energy radiation transport. In many cases, simpler and faster codes, which are far less costly and less time consuming to implement, may be used to adequately describe the transport. The precision of such codes may be evaluated by comparisons with equivalent Monte Carlo calculations, or with exact benchmark solutions (when they can be found). Once the mathematical precision of a particular code is established, the ultimate accuracy of its prediction will depend on the interaction cross-section data base used as input for calculations. Presently, nucleon (neutrons and protons) interaction cross sections are relatively well-known for wide ranges of energy and target materials. However, data are very limited for interaction cross sections for the 20–25 heavy-ion nuclei of importance for GCR exposure. Inevitably, data extrapolations and extensions by complex theoretical techniques are implemented in order to provide a comprehensive cross-section data base (Norbury and Townsend 1986; Townsend and Wilson 1985). This creates uncertainties in the transport calculations that are very difficult to quantify.

Radiobiology

Standard dosimetric techniques used to evaluate health risks due to radiation exposures are presently being challenged, particularly with regard to latent effects due to the high-energy, low-dose-rate exposure from the GCR heavy ions. Current methods for evaluating dose equivalents resulting from heavy-ion exposure utilize biological effectiveness quality factors (Q) that are specified as functions of linear energy transfer (LET) of the projectile particles to the biological system being traversed (ICRP-26, 1977). Predictions of the dose equivalent incurred in free space from GCR using the standard methods indicate that substantial shielding (20–50 g/cm^2) is required to reduce dose levels to an annual dose of 25–30 rem (Townsend et al. 1990a). Such shield amounts are very massive when large habitat modules are involved. Thus, efforts are in progress toward a better definition of risk assessment for GCR exposures. Newly proposed quality factors have been based on recent biological-effects data (ICRU-40, 1986). Preliminary calculations with the latest Q values indicate that previous evaluations may have been somewhat, but not dramatically, conservative (Wilson et al. 1990). Other recent studies have suggested abandoning the Q value/LET system (Katz 1986) and formulating more detailed models of cell destruction and transformation using radiosensitivity parameters derived from biological experiments (Cucinotta et al. 1991). Such direct biophysical models are expected to be a distinct improvement. However, the evolution of such models is directly coupled to the available radiobiological-effects data bases, which are very limited in number for GCR-type radiations. Clearly, the relationship between heavy-ion exposure and health risk is in need of better definition.

Dosimetric Measurement

The preceding discussion naturally leads to additional questions concerning measurement and monitoring of incurred radiation doses. Present space flight dosimetry instrumentation includes dosimeters of both thermo-luminescent and ionization chamber types, and they have been shown to be reliable and accurate for the Space Transportation System (STS) missions (Atwell 1990). In general, the STS dose rates are fairly low. For the 28.5° inclination orbits at altitudes between 250 and 350 km, the average dose rate is observed to be approximately 0.01 rad/day (or 3.6 rad/yr). Steady dose rates in free space, even with thick shields, are expected to be substantially higher (factors of 5 to 10), with intermittent (solar flare) dose rates higher still. Further advancement in dosimetric instrumentation and techniques will be required to monitor the astronaut free-space exposures, with emphasis on active, as opposed to passive, dosimeters. In particular, because the GCR interactions with thick shields may produce a high yield of neutrons, and precision in neutron dosimetry is currently considered to be rather poor (Paić 1988), improvements are certainly needed in this case.

Flare Prediction

The forecasting of large solar proton events is of vital importance for long-duration missions. Practically continuous monitoring of various aspects of solar activity (X rays and radio emissions, sunspot number, etc.) during solar cycle XXI (1975–1986) and up to the present time has provided a valuable data base for flare-forecasting statistics. The approach to flare forecasting used at the NOAA Space Environment Laboratory during recent years is to examine the intensities of X rays and radio emissions

and relate these to the likelihood of a subsequent energetic proton release. Estimates of the peak proton flux may also be made from these observations. For 24-hour predictions during solar cycle XXI, the number of events that occurred without prediction was about 10 percent of the total. This resulted primarily because the initial X rays and radio bursts were not on the visible portion of the Sun (Heckman et al. 1984). The false-alarm rate was approximately 50 percent, indicating that further work in this area is needed. Other techniques combine high-resolution observations of sunspot group patterns and magnetic field configurations in conjunction with H_α-line emission. Using these techniques, the prediction of occurrence is claimed to be up to several days in advance (Zirin and Liggett 1987). This method appears to show promise, but more observations are required to demonstrate the practicality of its implementation on a routine basis. For long-duration missions, additional onboard instruments for active proton detection should also be available to indicate when the use of a well-shielded storm shelter is warranted.

Alternate Shielding Concepts

Other topics of concern in the area of space radiation shielding include the effectiveness of material types (or the combination of material types) and alternate approaches to bulk shielding (e.g., magnetic and electromagnetic field deflection methods). As previously shown, recent results indicate that hydrogenous materials of low atomic weight are substantially superior to heavy metals for energetic ion shielding. However, little has been done in the study of the behavior of combinations, for example, alternating layers of light and heavy materials. Further studies should also address structural details of shields; in particular, corrugatedlike panels and/or shadow shielding techniques may offer advantages over simple wall structures. One recent study has indicated that magnetic shielding is of little use for protection from GCR (Townsend et al. 1990b). However, the Townsend study also showed that for representative large proton flares, great reductions in exposure can be achieved, and thus the potential use of magnetic shielding for flare protection may still be viable.

Concluding Remarks

Before astronaut dose estimates and subsequent shielding requirements can be determined for advanced lunar and Mars missions, many details of the missions must be specified. For instance, the following items must be defined in order to determine specific shielding requirements: the transfer vehicle configuration, the habitat configuration, the length of time required to shield habitats with regolith, the career limits of the crew, the year of the mission (solar minimum or maximum conditions), the duration of the mission, etc. Particular concerns for Mars mission planning include the following: whether any nuclear-powered propulsion is envisioned, the location of the habitat on the Martian surface, whether the crew will be spiraled through the Van Allen belts, etc. Estimates must also be made as to where the Mars crew will spend their time en route to Mars, i.e., how much of their time is anticipated to be spent in the more heavily shielded areas of the spacecraft as opposed to the less heavily shielded areas. Even with the specific details of the mission defined, the final shield design must consider the many uncertainties associated with current state-of-the-art radiation transport analyses.

Steps toward quantifying some of the issues involved with radiation protection for advanced lunar and Mars manned missions are presented in this report. After the definition of the galactic cosmic ray environment and the selection of various flare-environment scenarios, deterministic transport codes are used to determine the transport and attenuation of the free-space radiative fluxes through different media. From these basic propagation data, conservative dose estimates and shielding requirements are determined for simple-geometry transfer vehicles and for possible lunar/Martian habitat configurations. The results presented here are just part of the information required to determine radiation protection requirements for each phase of a complete mission scenario.

NASA Langley Research Center
Hampton, VA 23665-5225
December 17, 1990

References

Adams, J. H., Jr.; Silberberg, R.; and Tsao, C. H. 1981: *Cosmic Ray Effects on Microelectronics. Part I - The Near-Earth Particle Environment.* NRL Memo. Rep. 4506-Pt. I, U.S. Navy, Aug. (Available from DTIC as AD A103 897.)

Alred, J.; Bufkin, A.; Graf, J.; Kennedy, K.; Patterson, J.; Petro, A.; Roberts, M.; Stecklein, J.; and Sturm, J. 1988: Development of a Lunar Outpost: Year 2000-2005. *Lunar Bases and Space Activities in the 21st Century,* NASA, AIAA, Lunar & Planetary Inst., American Geophysical Union, American Nuclear Soc., American Soc. of Civil Engineers, Space Studies Inst., and National Space Soc., Paper No. LBS-88-240.

Atwell, William 1990: Astronaut Exposure to Space Radiation: Space Shuttle Experience. SAE Tech. Paper Ser. 901342, July.

Cucinotta, Francis A.; Katz, Robert; Wilson, John W.; Townsend, Lawrence W.; Nealy, John E.; and Shinn, Judy L. 1991: *Cellular Track Model of Biological Damage to Mammalian Cell Cultures From Galactic Cosmic Rays.* NASA TP-3055.

Dalton, Charles; and Hohmann, Edward, eds. 1972: *Conceptual Design of a Lunar Colony.* NASA CR-129164.

Feynman, Joan; and Gabriel, Stephen B. 1990: A New Model for Calculation and Prediction of Solar Proton Fluences. AIAA-90-0292, Jan.

Gaffey, John D., Jr.; and Bilitza, Dieter 1990: The NSSDC Trapped Radiation Model Facility. AIAA-90-0176, Jan.

Goswami, J. N.; McGuire, R. E.; Reedy, R. C.; Lal, D.; and Jha, R. 1988: Solar Flare Protons and Alpha Particles During the Last Three Solar Cycles. *J. Geophys. Res.,* vol. 93, no. A7, July 1, pp. 7195–7205.

Heckman, G.; Hirman, J.; Kunches, J.; and Balch, C. 1984: The Monitoring and Prediction of Solar Particle Events—An Experience Report. *Adv. Space Res.,* vol. 4, no. 10, pp. 165–172.

Recommendations of the International Commission on Radiological Protection 1977. ICRP Publ. 26, Pergamon Press, Jan. 17.

The Quality Factor in Radiation Protection 1986. ICRU Rep. 40, International Commission on Radiation Units and Measurements, Apr. 4.

Katz, Robert 1986: Biological Effects of Heavy Ions From the Standpoint of Target Theory. *Adv. Space Res.,* vol. 6, no. 11, pp. 191–198.

Kovalev, E. E.; Muratova, I. A.; and Petrov, V. M. 1989: Studies of the Radiation Environment Aboard Prognoz Satellites. *Nucl. Tracks Radiat. Meas.,* vol. 14, no. 1, pp. 45–48.

Maned-Systems Integration Standards 1987. NASA-STD-3000, Volume I, NASA Johnson Space Center, Mar.

Nagashima, K.; Sakakibara, S.; Murakami, K.; and Morishita, I. 1989: Response and Yield Functions of Neutron Monitor, Galactic Cosmic-Ray Spectrum and Its Solar Modulation, Derived From All the Available World-Wide Surveys. *Nuovo Cimento,* vol. 12C, ser. 1, no. 2, Mar–Apr., pp. 173–209.

National Council on Radiation Protection and Measurements 1989: *Guidance on Radiation Received in Space Activities.* NCRP Rep. No. 98, July 31.

Nealy, John E.; Wilson, John W.; and Townsend, Lawrence W. 1988: *Solar-Flare Shielding With Regolith at a Lunar-Base Site.* NASA TP-2869.

Nealy, John E.; Wilson, John W.; Townsend, Lawrence W. 1989: Preliminary Analyses of Space Radiation Protection for Lunar Base Surface Systems. SAE Tech. Paper Ser. 891487, July.

Nealy, John E.; Simonsen, Lisa C.; Townsend, Lawrence W.; and Wilson, John W. 1990: Deep-Space Radiation Exposure Analysis for Solar Cycle XXI (1975–1986). SAE Tech. Paper Ser. 901347, July.

Norbury, John W.; and Townsend, Lawrence W. 1986: *Electromagnetic Dissociation Effects in Galactic Heavy-Ion Fragmentation.* NASA TP-2527.

Paić, Guy, ed. c.1988: *Ionizing Radiation: Protection and Dosimetry.* CRC Press, Inc.

Parker, James F., Jr.; and West, Vita R., eds. 1973: *Bioastronautics Data Book,* Second ed. NASA SP-3006.

Sauer, Herbert H.; Zwickl, Ronald D.; and Ness, Martha J. 1990: *Summary Data for the Solar Energetic Particle Events of August Through December 1989.* Space Environment Lab., National Oceanic and Atmospheric Adm., Feb. 21.

Scott, W. Wayne; and Alsmiller, R. G., Jr. 1968: *Comparisons of Results Obtained With Several Proton Penetration Codes—Part II.* ORNL-RSIC-22, U.S. Atomic Energy Commission, June.

Shinn, Judy L.; Wilson, John W.; Nealy, John E.; and Cucinotta, Frances A. 1990: *Comparison of Dose Estimates Using the Buildup-Factor Method and a Baryon Transport Code (BRYNTRN) With Monte Carlo Results.* NASA TP-3021.

Simonsen, Lisa C.; Nealy, John E.; Townsend, Lawrence W.; and Wilson, John W. 1990a: *Radiation Exposure for Manned Mars Surface Missions.* NASA TP-2979.

Simonsen, Lisa C.; Nealy, John E.; Townsend, Lawrence W.; and Wilson, John W. 1990b: Space Radiation Shielding for a Martian Habitat. SAE Tech. Paper Ser. 901346, July.

Smith, Robert E.; and West, George S., compilers 1983: *Space and Planetary Environment Criteria Guidelines for Use in Space Vehicle Development, 1982 Revision (Volume 1).* NASA TM-82478.

Townsend, Lawrence W.; and Wilson, John W. 1985: *Tables of Nuclear Cross Sections for Galactic Cosmic Rays—Absorption Cross Sections.* NASA RP-1134.

Townsend, Lawrence W.; Nealy, John E.; Wilson, John W.; and Atwell, William 1989: Large Solar Flare Radiation Shielding Requirements for Manned Interplanetary Mission. *J. Spacecr. & Rockets,* vol. 26, no. 2, Mar./Apr., pp. 126–128.

Townsend, Lawrence W.; Nealy, John E.; Wilson, John W.; and Simonsen, Lisa C. 1990a: *Estimates of Galactic Cosmic Ray Shielding Requirements During Solar Minimum.* NASA TM-4167.

Townsend, L. W.; Wilson, J. W.; Shinn, J. L.; Nealy, J. E.; and Simonsen, L. C. 1990b: Radiation Protection Effectiveness of a Proposed Magnetic Shielding Concept for Manned Mars Missions. SAE Tech. Paper Ser. 901343, July.

Wilson, John W. 1977: *Analysis of the Theory of High-Energy Ion Transport.* NASA TN D-8381.

Wilson, John W. 1978: Environmental Geophysics and SPS Shielding. *Workshop on the Radiation Environment of the Satellite Power System,* Walter Schimmerling and Stanley B. Curtis, eds., LBL-8581 (Contract W-7405-ENG-48), Univ. of California, Sept. 15, pp. 33–116.

Wilson, John W.; and Badavi, F. F. 1986: Methods of Galactic Heavy Ion Transport. *Radiat. Res.,* vol. 108, pp. 231–237.

Wilson, J. W.; Townsend, L. W.; and Badavi, F. F. 1987: Galactic HZE Propagation Through the Earth's Atmosphere. *Radiat. Res.,* vol. 109, no. 2, Feb., pp. 173–183.

Wilson, John W.; and Townsend, L. W. 1988a: A Benchmark for Galactic Cosmic-Ray Transport Codes. *Radiat. Res.,* vol. 114, no. 2, May, pp. 201–206.

Wilson, J. W.; Townsend, L. W.; Buck, W. W.; Chun, S. Y.; Hong, B. S.; and Lamkin, S. L. 1988b: *Nucleon-Nucleus Interaction Data Base: Total Nuclear and Absorption Cross Sections.* NASA TM-4053.

Wilson, John W.; Townsend, Lawrence W.; Nealy, John E.; Chun, Sang Y.; Hong, B. S.; Buck, Warren W.; Lamkin, S. L.; Ganapol, Barry D.; Khan, Ferdous; and Cucinotta, Francis A. 1989: *BRYNTRN: A Baryon Transport Model.* NASA TP-2887.

Wilson, John W.; Shinn, Judy L.; and Townsend, Lawrence W. 1990: Nuclear Reaction Effects in Conventional Risk Assessment for Energetic Ion Exposure. *Health Phys.,* vol. 58, no. 6, June, pp. 749–752.

Zirin, Harold; and Liggett, Margaret A. 1987: Delta Spots and Great Flares. *Sol. Phys.,* vol. 113, nos. 1 & 2, pp. 267–283.

NASA
National Aeronautics and Space Administration

Report Documentation Page

1. Report No.	2. Government Accession No.	3. Recipient's Catalog No.
NASA TP-3079		

4. Title and Subtitle	5. Report Date
Radiation Protection for Human Missions to the Moon and Mars	February 1991
	6. Performing Organization Code
7. Author(s)	8. Performing Organization Report No.
Lisa C. Simonsen and John E. Nealy	L-16892
9. Performing Organization Name and Address	10. Work Unit No.
NASA Langley Research Center Hampton, VA 23665-5225	326-83-10-50
	11. Contract or Grant No.
12. Sponsoring Agency Name and Address	13. Type of Report and Period Covered
National Aeronautics and Space Administration Washington, DC 20546-0001	Technical Paper
	14. Sponsoring Agency Code

15. Supplementary Notes

16. Abstract

Radiation protection assessments are performed for advanced lunar and Mars manned missions. The Langley cosmic ray transport code and the Langley nucleon transport code are used to quantify the transport and attenuation of galactic cosmic rays and solar proton flares through various shielding media. Galactic cosmic radiation at solar maximum and minimum conditions, as well as various flare scenarios, is considered. Propagation data for water, aluminum, liquid hydrogen, lithium hydride, lead, and lunar and Martian regolith (soil) are included. Shield thickness and shield mass estimates required to maintain incurred doses below 30-day and annual limits (as set for Space Station *Freedom* and used as a guide for space exploration) are determined for simple-geometry transfer vehicles. Dose estimates are also presented for candidate lunar base habitats shielded with lunar regolith. On the surface of Mars, dose estimates are presented both for crews having the carbon dioxide atmosphere as their only protection and for crews protected by additional shielding provided by Martian regolith for a candidate habitat.

17. Key Words (Suggested by Authors(s))	18. Distribution Statement
Mars Moon Radiation Transfer vehicle Galactic cosmic rays Solar flares Manned missions	Unclassified—Unlimited Subject Category 93

19. Security Classif. (of this report)	20. Security Classif. (of this page)	21. No. of Pages	22. Price
Unclassified	Unclassified	25	A03

NASA FORM 1626 OCT 86

NASA-Langley, 1991

For sale by the National Technical Information Service, Springfield, Virginia 22161-2171